FORM TI-12
07/1999

B-T-3232

THE CORROSION BEHAVIOR OF HAFNIUM IN HIGH-TEMPERATURE-WATER ENVIRONMENTS

D. M. Rishel
J. D. Smee
B. F. Kammenzind

January 2000

DE-AC11-98PN38206

BETTIS ATOMIC POWER LABORATORY WEST MIFFLIN, PENNSYLVANIA 15122-0079

Operated for the U.S. Department of Energy
by Bechtel Bettis, Inc.

THE CORROSION BEHAVIOR OF HAFNIUM IN HIGH-TEMPERATURE-WATER ENVIRONMENTS

D.M. Rishel, J.D. Smee and B.F. Kammenzind

Abstract

The high-temperature-water corrosion performance of hafnium is evaluated. Corrosion kinetic data are used to develop correlations that are a function of time and temperature. The evaluation is based on corrosion tests conducted in out-of-pile autoclaves and in out-of-flux locations of the Advanced Test Reactor (ATR) at temperatures ranging from 288°C to 360°C. Similar to the corrosion behavior of unalloyed zirconium, the high-temperature-water corrosion response of hafnium exhibits three corrosion regimes: pretransition, posttransition, and spalling. In the pretransition regime, cubic corrosion kinetics are exhibited, whereas in the posttransition regime, linear corrosion kinetics are exhibited. Because of the scatter in the spalling regime data, it is not reasonable to use a best fit of the data to describe spalling regime corrosion. Data also show that neutron irradiation does not alter the corrosion performance of hafnium. Finally, the data illustrate that the corrosion rate of hafnium is significantly less than that of Zircaloy-2 and Zircaloy-4.

1. Introduction

The US Department of Energy (DOE) has been tasked with the establishment of a long-term disposal capability of spent fuel from nuclear reactors. The primary function of the repository is to ensure that the environment is protected by delaying and controlling the release of radioactive material. Initially, disposal canisters will provide the primary barrier to the release of radioactive material. In addition to the disposal canisters, Zircaloy fuel cladding provides a significant additional barrier for Naval fuel. Hillner et al. [Reference (1)] recently reported on Zircaloy corrosion based on long-term Zircaloy autoclave corrosion data. These data were used to estimate the amount of corrosion that may be experienced by spent Zircaloy-clad fuel assemblies during long-term exposure to geologic repository conditions.

To ensure adequate reactivity control, hafnium may be inserted into fuel assemblies. In some cases, this hafnium could be irradiated. As is the case for Zircaloy cladding [Reference (1)] it is important to understand the corrosion behavior of Hf. Compared to the Zircaloys, there is little hafnium corrosion data in the open literature. Most of the hafnium corrosion data reported have been obtained at temperatures greater than 350°C in gaseous environments such as oxygen, air, or steam, [References (2-5)]. Smeltzer and Simnad [Reference (5)] systematically determined the reaction kinetics of hafnium in pure dry oxygen. In that study, hafnium crystal bar material containing up to 5.0 w/o Zr was used. Gravimetric measurements were made at an oxygen pressure of 760 mm Hg at temperatures ranging from 350°C to 1,200°C.

Smeltzer and Simnad, [Reference (5)], found that the following logarithmic, parabolic, and linear rate equations represented their data for the temperature ranges of 350°C-710°C, 470°C-1,200°C and 900°C-1,200°C, using activation energies of 47.6 kJ, 150.4 kJ, and 109.0 kJ, respectively.

$$\Delta W' = 2\ x\ 10^{-2}\left(\exp\frac{-47{,}630}{RT}\right)\ln\left[1+\left(7.7\left(\exp\frac{-22{,}562}{RT}\right)\right)t\right], \qquad (1)$$

$$(\Delta W')^2 = \left(6x10^{-2}\exp\frac{-150{,}411}{RT}\right)t + a(T), \qquad (2)$$

and

$$\Delta W' = \left(6x10^{-2}\ \exp\frac{-109{,}048}{RT}\right)t + b(T) \qquad (3)$$

where $\Delta W'$ is the oxygen weight gain in units of gm/cm^2, t is the time in minutes, R is the gas constant (in Joules/mol/°K), T is the temperature in °K, and a and b are temperature-dependent constants. The logarithmic and parabolic empirical relationships are correlated with the formation of compact oxides, while the linear rate empirical relationship is associated with a layered porous scale. Parabolic

oxidation behavior obeys the Wagner theory of oxidation, which for hafnium oxidation occurs with the inward diffusion of oxygen as ions, via anion vacancies, to react with hafnium at the metal/oxide interface [Reference (6)]. The mechanisms associated with the logarithmic relationship are not as well established but are interpreted to be based on the adsorption of reactive species, the effects of electric fields across oxide layers, quantum-mechanical tunneling of electrons through thin scales, progressive blocking of low-resistance diffusion paths, nonisothermal conditions in the oxide layer, and nucleation and growth processes [Reference (6)]. The linear rate relationship expression may reflect a reaction that is controlled by diffusion through a thin inner layer of the oxide that is maintained at a constant thickness with time due to repetitive delamination or exfoliation of hafnium oxide. Alternatively, the linear rate relationship may reflect a rate-determining phase boundary process, e.g., nucleation and growth of the oxide [Reference (7)].

There are a few reports describing the corrosion response of hafnium under aqueous environments. In these studies the reported information describes the corrosion behavior of hafnium under a specific set of conditions. For example, in Russian WWER-1000 pressurized water reactors, it has been reported [Reference (8)] that hafnium has been considered for use as neutron absorbing components. Corrosion test results indicate that under conditions corresponding to WWER-1000 primary circuit water, the corrosion resistance of pure hafnium is very high; [In WWER-1000 PWRs the inlet and outlet water temperatures are 290°C and 320°C, respectively]. Furthermore, under irradiation hafnium was reported to retain its high corrosion resistance. After 26,800 hours at operating conditions, a dense oxide film, 5-20 μm thick formed, for which the corrosion rate was essentially zero after the first 4,000 hours of operation. In Japan, hafnium is one material being used in advanced control rods for BWR plants [Reference (9)]. One reason for the selection of hafnium is its superior corrosion performance. Corrosion test results in steam at 500°C and 10.5 MPa found that although hafnium undergoes nodular corrosion, it exhibits superior corrosion performance to that of Zircaloy-4. The addition of small amounts of iron improved resistance to nodular corrosion [Reference (9)].

The properties of Shippingport PWR hafnium control rods were reported in References (10) and (11). The corrosion film thicknesses formed on the surface of a control rod that had experienced up to 1100 days of exposure (21,035 effective full power hours (EFPH)) at temperatures of approximately 280°C were found to range in thickness from 0.16 μm to 0.34 μm [Reference (11)]. The oxide-film thicknesses of all irradiated hafnium material taken from this control rod were very similar. There were essentially no differences among sections exposed to thermal neutron fluences ranging from 4.5×10^{20} nvt to 7.4×10^{20} nvt, and fast neutron (>1 MeV) fluences ranging from 36×10^{20} nvt to 54×10^{20} nvt.

The examples cited above suggest that hafnium has a high resistance to corrosion; however, there are little published corrosion data from systematic studies to use in aqueous corrosion rate correlations. The use of the available published kinetic data obtained from elevated temperature experiments conducted in gaseous environments in predicting the corrosion behavior of hafnium at lower temperatures in aqueous environments requires significant extrapolations due to the vastly different environmental conditions. Lower-temperature water corrosion data would reduce the extrapolation. To provide a basis for evaluating the corrosion behavior of hafnium in a repository environment, correlations of hafnium corrosion are developed from corrosion data generated by the Bettis Atomic Power Laboratory in high-temperature-water environments. These data were generated from tests that have been conducted over the last twenty-five years with accumulated exposure times up to sixteen years. The results of this analysis are presented below.

2. Experimental

2.1 Specimens

Corrosion tests were conducted on fully annealed and recrystallized specimens fabricated from material that meets or exceeds the chemical composition of ASTM B 776, nuclear grade (R1) hafnium. Corrosion specimens were made from nine different ingots, for which the compositions are listed in Table 1. The corrosion data were obtained with specimens of three different sizes (Table 2). In addition, four different prefilm conditions (Table 3) were tested. Prior to prefilming or testing (in the case for specimens tested without any prefilm), the specimens were pickled to a bright surface finish in a bath comprised of approximately 39 v/o nitric acid, 3 v/o hydrofluoric acid and the balance water. The specimens were pickled long enough to ensure that approximately 50 microns of material were removed per surface.

2.2 Corrosion Tests

Isothermal corrosion tests were conducted either in static autoclaves or in flowing test loops in the Advanced Test Reactor (ATR) in out of neutron flux (OOF) positions[1]. Corrosion data were obtained from fifteen autoclave and twelve ATR tests that included a total of 129 coupons. The autoclave tests were conducted at one of four nominal temperatures; 288°C, 316°C, 338°C, and 360°C. The ATR tests were conducted at one of three nominal temperatures; 310°C, 332°C, and 354°C. All tests, in both the static autoclaves and ATR, were conducted under subcooled, pressurized water conditions. A summary of the materials and test conditions that were evaluated is provided in Table 4. With two

[1]Although other hafnium coupons were exposed to neutron fluxes, corrosion data could not be obtained via weight gain measurements due to the fact that the most significant contributor to the observed weight gain would have been caused by neutron absorption.

exceptions, all tests were conducted in water in which 1) the room-temperature pH was maintained between 10.1 and 10.3, 2) the oxygen content was less than 20 ppb, 3) the hydrogen content was maintained between 10 cc H_2/kg H_2O and 60 cc H_2/kg H_2O and 4) the conductivity was maintained between 20 μS/cm to 80 μS/cm. Tests numbered 5 and 6 were conducted in deionized, degassed water, at a room-temperature pH of 7. During the course of the corrosion tests, the corrosion coupons were periodically weighed to determine the corrosion weight gains. Hafnium is such a corrosion resistant material that the magnitudes of weight gain measurements are very small. A weight gain of 1 mg/dm^2 corresponds to a weight increment on the specimen of approximately 0.1 mg. As the data were obtained with four-place balances, measurements were of the same order of magnitude as the uncertainty in the balance.

3. Results and Model Development

3.1 Observed Behavior

Hafnium is in the same group in the periodic table as zirconium, and like zirconium it forms only one stable oxide, HfO_2. In water, the formation of the corrosion film, HfO_2, can be described by the following reaction:

$$Hf + 2H_2O = HfO_2 + 2H_2 \qquad (4)$$

Assuming that all the oxygen generated via Equation (4) reacts with hafnium to form a uniform, adherent, stoichiometric, non-porous oxide layer, the oxide film thickness can be estimated from the weight gain of the corrosion specimen[2]. During the course of each test, periodic weight measurements were recorded. The data for each of the tests listed in Table 4 are tabulated in the Appendix.

An example of the hot-water corrosion behavior of hafnium is illustrated in Figure 1 for samples exposed in an autoclave at 360°C in pH 10 water. In the first approximately 500 days of testing, the weight changes are relatively small and well behaved, implying that the oxide scale is adherent and protective. Over the subsequent 1700 days of testing, a significant range of variability and increase in data scatter is observed. The weight loss is caused by spalling, and the variability in weight change results from the variation in spalling with time. The behavior shown in Figure 1 is typical of the corrosion behavior that was observed at other temperatures in both autoclave and ATR test environments. Based upon the test data presented in Table 4 and the Appendix, the hot-water

[2] 14.7 mg/dm^2 of weight gain = 1 μm of oxide growth = 0.6 μm of metal consumed.

corrosion of unalloyed hafnium displays three distinct kinetic regimes, and two distinct transition points. These regimes and transition points are schematically illustrated in Figure 2 and are described as follows:

1. During the first regime, the oxide film weight-gain rate decreases with exposure. This suggests that the oxide film serves as a protective adherent barrier to the further corrosion of the hafnium metal substrate. Visually, the corrosion coupons exhibit a multicolored, iridescent, semitransparent film in the early stage of exposure. The color changes to a lustrous black in the later stage. The oxide film in this regime grows approximately in accordance with a cubic rate relationship. The regime is referred to as the pretransition regime.

2. The pretransition and posttransition regimes are separated by the first transition point or transition time.

3. In the posttransition regime the corrosion kinetics are best described as linear. That is, the corrosion rate is constant. The oxide film exhibits a combination iridescent, semigloss light gray finish.

4. The second transition demarks the start of the oxide spalling regime.

5. The spalling regime is characterized by weight loss and a significant amount of weight-change variability. The corrosion film in this regime exhibits a matte gray appearance and is powdery and can be removed with minimal effort. In this regime small levels of spalling can result in relatively large changes in weight change. This is because weight gains involve only the uptake of oxygen, whereas weight loss involves both oxygen and hafnium (in the form of HfO_2) and the fact that hafnium is much heavier than oxygen. For example, a weight loss of 10 mg/dm^2 from a sample that had a corrosion weight gain of 10 mg/dm^2 would require only 15 percent of the oxide film to have spalled from the surface. Scanning electron microscopy has shown that hafnium oxide spalling consists of a fracturing of the oxide into small pieces.

With the exception of the magnitude of the weight gains being less, the corrosion behavior of hafnium in high-temperature water between the temperatures of 260°C to 360°C is very similar to that of crystal-bar zirconium [Reference (12)]. In early stages of exposure, crystal-bar zirconium develops a lustrous black, tightly adherent corrosion film. At some point during the exposure, a rapid increase in the corrosion kinetics is observed with crystal-bar zirconium, coincident with the formation of a white corrosion product, which is followed shortly by the loss of oxide through spalling.

3.2 Method of Data Analysis

Some samples had oxide films, i.e., prefilms, at the start of the tests and some did not. To take into account the effect of prefilming, adjustments were made to the specimen exposure times. This was done to effectively reference the start of each test at time, t = 0. Using an initial estimate of the pretransition corrosion rates, which were later refined by iteration, the number of equivalent days of exposure at any given test temperature was calculated from the average prefilm weight. For specimens in which no prefilms were applied, no adjustments were made to their exposure times.

The corrosion kinetic data obtained from each of the tests were analyzed to determine best-fit correlations in both the pretransition and posttransition corrosion regimes. In addition, the times to the first transition (TTT) were correlated as a function of temperature. The analyses were conducted using a variety of software packages. The SOLO statistical software package was used to determine the delineation between the pretransition and posttransition regimes, i.e., the times to transition, whereas LOTUS 1-2-3 and SigmaPlot 4.0 were used to determine the best-fit correlations of corrosion weight gain as a function of exposure time. In each of the tests as identified in Table 4, correlated fits were made through the averaged weight gain data for each time interval. The pretransition correlations were made on measurements obtained prior to the time-to-transition, whereas the posttransition correlations were made on measurements obtained between the time to transition and the onset of spalling as indicated by weight losses. The method by which the time to transition, which delineates the pretransition and posttransition corrosion regimes, was obtained is described below.

In general, at any given temperature, the kinetics of corrosion can be described by the empirical equation, $\Delta W^n = k\,t$, where ΔW is the weight gain per unit area of the original surface in units of mg/dm^2, t is the exposure time in days, and n and k are constants for a given temperature [Reference (13)]. When n is equal to 3, the rate equations are said to be cubic; when n is equal to 2, the rate equation is said to be parabolic, and when n is unity, linear kinetics occur. In the last case, the oxidation process is considered to be nonprotective. As the protective nature of the oxide increases, the value of the exponent n increases. In the correlations described below, only corrosion-kinetic data that are in the pretransition and posttransition corrosion regimes are evaluated. Data that are within the spalling regime are excluded from the analysis.

Pretransition Correlations

The pretransition corrosion kinetics at a given temperature are approximated by the general equation $\Delta W = k_{c'} t^{1/n}$, where $k_{c'}$ is an empirical constant, which is termed the pretransition rate constant, and n is a constant that is greater than 2. The constants of the applicable rate equations are determined by using the logarithmic form, $\log \Delta W = \log k_{c'} + 1/n \log t$. A plot of ΔW against time t on logarithmic coordinates yields a straight line having a slope of $1/n$.

Values of $k_{c'}$ and $1/n$ are determined for each test from the data that are within the pretransition regime. The values of the best fit pretransition rate constants, $k_{c'}$, and exponents n, along with the times to transition are listed in Table 5. The exponents n ranged from 2.60 to 3.63, averaged 3.08, and did not appear to be a function of temperature. In developing a correlation to be used for engineering purposes, it is assumed that the exponent is a constant, and that the best fit is a cubic correlation, (i.e., n = 3), for each of the tests evaluated. Based on a value of n equal to 3, each of the coefficients $k_{c'}$ were normalized. This normalization was done by forcing the correlation for each test to fit through the averaged coupon weight gain at the last examination time in the pretransition regime. The resulting normalized coefficients, $k_{c'}$, also are listed in Table 5.

The corrosion-kinetic variation with temperature is modeled as a multiplier, i.e., rate constant to the time variable. The resulting equation, as a function of temperature, is of the form $k_c = A_c e^{-Q_c/T}$. The values of A_C and Q_C are determined by a least squares linear regression analysis, Figure 3, of the natural logarithm of the cube, of $k_{c'}$ *(Note :* $(k_{c'})^3 = k_c$*)*, of the pretransition hafnium corrosion rate constants (from each test) vs. inverse temperature (°K), (weighted by the number of corrosion coupons). The resultant correlations obtained are;

$$\Delta W^3 = \left(5.65 \times 10^{12}\right) \exp\left(\frac{-17{,}883 \pm 995}{T}\right) t, \quad \left(\frac{mg}{dm^2}\right)^3 \tag{5}$$

$$\Delta W = \left(1.78 \times 10^{4}\right) \exp\left(\frac{-5{,}961 \pm 332}{T}\right) t^{1/3}, \quad \left(\frac{mg}{dm^2}\right) \tag{6}$$

From Equation (5) an activation energy, Q, of 148.3 kJ/mole is obtained.

Posttransition Correlations

Data in the posttransition corrosion regime are described by linear corrosion kinetics. That is, $\Delta W = k_L t$, where k_L is in units of mg/dm^2/day and is termed the linear rate constant. Values of k_L are determined from each test, (with the exception of Tests Nos. 6, and 23, 24, 25 and 26, in which insufficient data exist to support estimating k_L, for the posttransition correlation), and are listed in Table 6. As is the case for the pretransition corrosion regime, the corrosion kinetic variation with temperature is modeled as a multiplier to the time variable, i.e., $k_L = A_L e^{-Q_L/T}$. In Figure 4 the natural logarithm of the linear rate constant vs. inverse temperature (°K) is plotted. Based on a linear regression analysis, the following correlation is obtained,

$$\Delta W = \left(2.00\, x\, 10^{6}\right)\exp\left(\frac{-11{,}133 \pm 860}{T}\right)t, \quad \left(\frac{mg}{dm^2}\right) \tag{7}$$

From Equation (7), an activation energy of 92.6 kJ/mol is derived.

Time to Transition, TTT

As shown above, the corrosion of hafnium is characterized by the initial formation of a thin, iridescent, tightly adherent oxide film, corresponding to an approximately cubic rate relationship behavior up to a weight gain of 7 mg/dm^2 to 10 mg/dm^2 (0.5 μm to 0.7 μm of oxide). Further exposure beyond this point produces linear kinetics. The point on the corrosion weight gain curve where the cubic and linear portions of the corrosion kinetics curve intersect is termed "transition" [Reference (12)]. In determining the time to transition, use was made of the fact that, at any given temperature and pH, the tests listed in Table 4 were conducted in the same autoclave or ATR loop. Thus, the tests described in Table 4 were catergorized into groups. For each group[3], the averaged weight gain vs. time data (for each of the tests within that group) were incorporated into a single spreadsheet file and analyzed using the SOLO statistical software package. From this method of grouping and analysis, the time-to-transition data listed in Table 5 were obtained.

A plot of the natural log of the time to transition values, as listed in Table 5, versus inverse temperature is shown in Figure 5. The expression for the time to transition correlation plotted in Figure 5 is,

$$TTT = \left(4.68\, x\, 10^{-9}\right)\exp\left(\frac{15{,}415 \pm 1{,}494}{T}\right), \quad (Days) \tag{8}$$

[3] For any given group of tests, the materials were obtained from the same ingot and exposed under the same conditions, i.e., temperature and pH. The only difference between each of the tests within any for any given group was in the oxide prefilms that had been applied prior to testing.

3.3 Metallography

To illustrate the nature of the oxide films that formed on hafnium in the pretransition, posttransition, and spalling regimes, corrosion coupons from each of these regimes were examined. The nature and thickness of the oxide films that was observed on these coupons is typical of oxide films that have been observed on Hf from over twenty-five years of testing. The corrosion coupons that were examined were removed from 360°C, pH 7 autoclave tests. Scanning electron microscope (SEM) examinations of both the surface of the oxide layer and its cross-section were performed. Prior to examining the surface of the oxide layer a conductive gold coating was applied. The specimens were sectioned and mounted in a hot press. Prior to mounting, an aluminum foil layer was wrapped around the specimen to improve the oxide edge retention. The specimens were ground to remove approximately 500 μm of material on a Petrodisc-M wheel with a slurry comprised of 15 μm diamond abrasive and Struers DP-Green lubricant. Rough polishing was performed in two steps by first using a DP-Plan fine grinding nylon cloth with a 15-μm diamond suspension, which was then followed by a polish using a met cloth with 6-μm diamond paste. Final polishing was performed using a microcloth with Linde B and an acid polish solution consisting of 870 ml H_2O, 10 ml HF (49 wt%), 20 ml HNO_3 (70 wt%) and 100 gms Oxalic acid (98 wt%). The purpose of the acid polish solution was to prevent smearing of the metal during the final polishing step. To reveal the grain boundaries in the metal substrate, the specimens were swab etched using a solution comprised of 60 ml H_2O_2 (30 wt%), 30 ml HNO_3 (70 wt%), 30 ml ethanol and 2 drops of HF (49 wt%).

Pretransition Oxide

A sample that had attained a final weight gain of 6.2 mg/dm^2, after 125 days at 360°C, was removed from autoclave testing. This coupon was expected to exhibit cubic pre-transition corrosion kinetics since at 360°C the predicted time to transition (per Eqn. (8)) was 174 days. To the eye, the oxide exhibited red, blue, and green iridescence. The surface as seen with the SEM is shown in Figure 6. In general, the surface is smooth and planar. A network of what appear to be defects is observed to snake through the smooth oxide layer. At higher magnification, these defects are observed to be areas where the oxide has locally cracked. From the size and shape of the pattern produced, the network of cracks appears to follow grain boundaries in the original metal surface. No spalling is observed.

A cross-sectional view of the oxide formed is shown in Figure 7. For the most part the oxide has a uniform thickness of approximately 0.4 μm; (Note: Based on Eqn. (6), a weight gain of 7.33 mg/dm^2 and an oxide thickness of 0.50 μm would have been predicted). However, there are instances where, in cross section, nodular-like features are observed. The oxide associated with these features protrudes above the surface of the uniform oxide and penetrates into the Hf substrate. The oxide

associated with these nodule-like features is on the order of 1 to 2 μm thick. These local penetrations of oxide appear to correspond to the network of cracks and defects observed in the planar examination.

Posttransition Oxide

Another coupon was removed from autoclave testing after 540 days at 360°C. It had attained a final weight gain of 15.1 mg/dm^2. This coupon was expected to exhibit linear posttransition corrosion kinetics. Visually, the oxide surface was light gray in appearance with some evidence of iridescence. The surface SEM examination of this coupon, see Figure 8, found that a network of defects existed, which were more pronounced than the cracks observed for the 125-day coupon shown in Figures 6 and 7. The oxide along this network was rough and exhibited evidence of oxide spalling. Within the fractured network were islands of oxide that appeared relatively smooth. These areas are probably regions covered by a thin, uniform, adherent oxide.

As shown in Figure 9, a cross-sectional SEM examination of this coupon found that for the most part this coupon is covered by an adherent corrosion film that was quite thin, measuring less than 1 μm in thickness. In addition to the thin adherent oxide, there were regions in which the nodular-like oxide existed. In contrast to the pretransition regime, the nodular-like features were observed to be both more frequent and had penetrated deeper (up to 5 μm) into the hafnium metal substrate. Relating the surface micrographs of Figure 8 to the cross-sectional micrographs of Figure 9, the regions surrounded by the fractured network of oxide correspond to the thin adherent portion of the oxide film. On the other hand, the fractured network observed in Figure 8 corresponds to the nonuniform fractured oxide layers observed in Figure 9. Figure 10 shows this coupon after having been etched to reveal the grain boundary structure. This micrograph illustrates that the nodule-like oxide features penetrate the hafnium metal substrate at grain boundaries.

Spalling Oxide

A coupon that demonstrated oxide spalling is shown in Figure 11. This coupon had been exposed for 731 days at 360°C and exhibited a weight loss of 26.7 mg/dm^2. The oxide layer was off-white in color. Powdery white oxide was easily removed by rubbing. Micrographs of the surface oxide layer are observed and illustrate that the majority of the coupon surface is rough and uneven. However, within the rough regions there are islands of oxide which appear relatively smooth. It is likely that these regions correspond to portions of the oxide layer that are thin, uniform, and adherent.

In cross-section (Figure 12) the majority of the coupon surface is seen to be covered by a fractured, multilayered oxide film, with each layer tending to be on the order of 1 μm or less. In addition, the

layered structures of these oxide regions that are spalling appear to be more loosely connected than those in oxides that do not appear to be spalling. This suggests that the layer boundaries are fracture planes for the spalling process.

In summary, the metallograhic examinations have ascertained that in the pretransition regime, where cubic corrosion kinetics are exhibited, a thin (< 1 μm), adherent, protective oxide layer exists. The onset of the posttransition corrosion regime, where linear corrosion kinetics are observed, occurs as a result of the localized breakdown of the oxide film into a nodular-like oxide film. The breakdown of the oxide film is associated with the hafnium metal grain boundaries. As the spalling regime is entered, the nodular-like features grow in size, both laterally along the oxide surface and in depth into the metal substrate. Their growth corresponds to an increasing percentage of the total specimen surface. Due to its friable nature, the oxide film is susceptible to a powdery form of spalling, and weight losses occur.

3.4 Hf vs. Zircaloy Corrosion Rate Comparison

The corrosion rate of hafnium is less than that for Zircaloys. With the use of Equations (6-8), this difference in corrosion performance can be quantified. Use was made of the relationships presented by Hillner in Reference (12) in comparing the pretransition, posttransition and time-to-transition behavior. The ratios of the relevant Hf to Zircaloy rate equations are summarized in Table 7 for two temperatures, 100°C and 310°C. The data in this table illustrate that in both the pretransition and posttransition corrosion regimes, the corrosion resistance of hafnium is significantly greater than that of Zircaloy. In addition, the time to transition of hafnium is longer than that for Zircaloy, e.g., at least 2.5 times greater at 310°C, and increases as temperature decreases.

3.5 Influence of Irradiation on Corrosion

Comparisons of the in-reactor corrosion behavior of the Zircaloys with the out-of-reactor or ex-reactor corrosion behavior show that corrosion is enhanced by neutron irradiation [Reference (14)]. For hafnium, data that show the effect of irradiation on corrosion behavior are more limited. Irradiation is expected to affect the corrosion behavior of hafnium in two ways. First, the corrosion product film, when subjected to a neutron flux, is expected to receive some form of radiation damage (e.g., via atom displacements) that could enhance corrosion. Second, due to its large neutron absorption cross-section, the resulting transmutation products of hafnium may affect its corrosion behavior. Naturally occurring hafnium is composed of six stable isotopes: ^{174}Hf, ^{176}Hf, ^{177}Hf, ^{178}Hf, ^{179}Hf, and ^{180}Hf. Tantalum, a major transmutation product is formed via the (n,γ) reaction of ^{180}Hf followed by the β^- decay of ^{181}Hf to the stable ^{181}Ta isotope. Tungsten and lutetium also are produced, but in much smaller quantities. For the control rod exposed during three seed lives in PWR Core 1, [Reference

(11)], tantalum and lutetium analyses were performed as a function of depth below the surface in regions that had been subjected to a radially (as referenced from the core center) averaged thermal neutron fluence of 4.17×10^{20} nvt to 11.6×10^{20} nvt; (the radially averaged fast fluence (> 1 MeV) ranged from 37×10^{20} nvt to 54×10^{20} nvt). This analysis showed that the tantalum and lutetium concentrations are, in general, higher near the material surface and are proportional to neutron fluence (Table 8).

Corrosion During Irradiation

Due to the confounding effect of neutron absorption on corrosion weight gain measurements, the impact of irradiation on corrosion can only be ascertained through oxide thickness measurements, as obtained via destructive examination. Thus the amount of data available is more limited as compared to weight change data. In-reactor data that have been obtained through destructive metallographic examinations are presented in Table 9. In this table the average metallographically measured oxide thickness is compared with the range of oxide thicknesses as predicted by the out-of-pile pretransition weight gain correlation, Equation (6).

The following conclusions are drawn from these comparisons. First the in-flux measured oxide thicknesses fall within the expected range of values predicted for pretransition corrosion kinetics, as correlated from the autoclave and out-of-flux studies; therefore, it is concluded that corrosion is not accelerated by irradiation. Second, the increase in tantalum buildup has no effect upon the corrosion rate. Based on these observations, it is expected postirradiated corrosion within the pretransition regime would be unaffected by prior irradiation. Data that would illustrate the effect of irradiation on posttransition corrosion behavior are not available.

4. CONCLUSION

High-temperature water corrosion data for hafnium has been evaluated. Hafnium is observed to exhibit pretransition, posttransition, and spalling corrosion regimes. For the pretransition and posttransition regimes, correlations are developed that are functions of time and temperature. For the pretransition regime, cubic corrosion kinetics are observed, whereas in the posttransition regime, linear corrosion kinetics are observed. The data show that for the pretransition and posttransition regimes, hafnium is more corrosion resistant than zirconium or the Zircaloys. Metallography has determined that a thin, protective oxide layer is formed during the pretransition regime. The onset of the posttransition regime and the progression into the spalling regime are associated with the breakdown and loss of the oxide film from regions at hafnium metal grain boundaries. The correlations that are derived may be used as a basis for estimating the amount of corrosion that occurs on hafnium stored in a repository. Neutron irradiation does not adversely affect the corrosion performance of hafnium.

ACKNOWLEDGMENTS

The authors wish to acknowledge the direction supplied by, and the many helpful discussions held with Dr. D. G. Franklin. The aid of Mr. W. A. Meyer in providing correlations of the kinetic data and Messrs. D. M. Gasparovic, G. A. Hoffman, and B. J. Whitmore in assisting with the metallographic examinations is acknowledged. The information provided by Messrs. P. M. Rosecrans and D. J. Sepe, of Knolls Atomic Power Laboratory are appreciated. Finally, the helpful comments of Mr. R.F. Beyer are recognized.

References

(1) Hillner, E., Franklin, D.G., and Smee, J.D., "The Corrosion of Zircaloy-Clad Fuel Assemblies in a Geologic Repository Environment," WAPD-T-3173, September 3, 1997.

(2) Pemsler, J.P., "Studies on the Oxygen Gradients in Oxidizing Metals II. Hafnium," J. Electrochem. Soc., 111, p. 1067, (1958).

(3) Pemsler, J.P., "Diffusion of Oxygen in Hafnium," J. Electrochem. Soc., 111, p. 1185, (1964).

(4) Gadd, J.D., and Evans, E.B., "High Temperature Scaling of Hafnium in Air," Corrosion, 17, p. 109, (1961).

(5) Smeltzer, W.W. and Simnad, M.T., "Oxidation of Hafnium," Acta. Met., 5, pp. 328-334, (1957).

(6) Birks, N. and Meier, G.H., "Introduction to High Temperature Oxidation of Metals," pp. 41-62, Edward Arnold, London, 1983.

(7) Kofstad, P., "High Temperature Corrosion", pp. 278-308, Elsevier Applied Science, New York, 1988.

(8) Chernishov, V.M., and Vasilchenko, I.N., "Control Members of WWER-440 and WWER-1000 Power Reactors," in "Proceedings, IAEA Technical Committee Meeting on Advances in Control Assembly Materials for Water Reactors," International Atomic Energy Agency, Vienna, IAEA-TECDOC-813, pp. 105-120, 1993.

(9) Shirayanagi, H., Fukumoto, T. and Shiga, S., "Advanced Control Rods for Japanese BWR Plants," in "Proceedings, IAEA Technical Committee Meeting on Advances in Control Assembly Materials for Water Reactors," International Atomic Energy Agency, Vienna, IAEA-TECDOC-813, pp. 135-164, 1993.

(10) Salvaggio, G.J., Nichols, F.A., and Bacca, J.P. Jr., "Properties of a Hafnium Control Rod After Exposure During Two Seed Lives in PWR Core 1," WAPD-TM-337, November 1962.

(11) Salvaggio, G.J., Weinberg, J.G., Kass, S. and Longua, K.J., "Properties of a Hafnium Control Rod After Exposure During Three Seed Lives in PWR Core 1," USAEC Report WAPD-TM-457, U.S. Atomic Energy Commission, Bettis Atomic Power Laboratory, June 1965.

(12) Hillner, E., "Corrosion of Zirconium-Base Alloys - An Overview," in "Zirconium in the Nuclear Industry, ASTM STP 633, A. L. Lowe, Jr. and G.W. Parry, Eds., American Society for Testing and Materials," pp. 211-235, (1977).

(13) Hillner, E., "The High-Temperature Oxidation Kinetics of Zirconium in Dry Oxygen," in Zirconium and its Alloys, The Electrochemical Society, pp. 132-137, (1966).

(14) Stehle, H., Garzarolli, F., Garde, A.M., and Smerd, P.G., "Characterization of ZrO_2 Films Formed In-Reactor and Ex-Reactor to Study the Factors Contributing to the In-Reactor Waterside Corrosion of Zircaloy," in "Zirconium in the Nuclear Industry: Sixth International Symposium, ASTM STP 824". D.G. Franklin and R.B. Adamson, Eds., American Society for Testing and Materials, pp. 483-506, 1984.

Table 1
Ingot Composition
(In ppm unless otherwise indicated)

Element	Ingot A	Ingot B	Ingot C	Ingot D	Ingot E
Hf (wt %)	>95.3	>95.3	>95.3	>95.3	>95.3
Fe	82 – 138	173 - 186	152 - 169	139 - 166	179 – 190
O	180 – 280	170 - 190	170 - 190	220 - 250	170 - 200
Al	<50	<50	<50	<50	<50
C	30	50	<30	40 - 50	<30
Cu	<50	<50	<50	<50	<50
H	<5	6	7	7	<5
Mo	<10	<10	<10	<10	<10
N	22	19 - 20	24 - 27	15 - 23	17
Nb	<50	<50	<50	<50	<50
Ta	<100	<100	<100	<100	<100
Ti	<50	<50	<50	<50	<50
U	0.92	1.12	1.21	0.87	0.84
W	<75	<75	<75	<75	<75
Zr (wt %)	2.53 – 2.61	2.64 – 2.86	2.77 – 2.83	3.17 – 3.23	2.94 – 3.01
B	<0.5	<0.5	<0.5	<0.5	<0.5
Cd	<2.5	<2.5	<2.5	<2.5	<2.5
Co	<5	<5	<5	<5	<5
Cr	<100	<100	<100	<100	<100
Gd	<2.5	<2.5	<2.5	<2.5	<2.5
Mn	<25	<25	<25	<25	<25
Ni	<25	<25	<25	<25	<25
P	<3	<3	<3	<3	<3
Pb	<10	<10	<10	<10	<10
Si	<25	26	28	<25	35
Sn	<10	<10	<10	<10	<10
Th	<3.5	<3.5	<3.5	<3.5	<3.5
V	<25	<25	<25	<25	<25

Table 1 (continued)
Ingot Composition
(In ppm unless otherwise indicated)

Element	Ingot F	Ingot G	Ingot H	Ingot I
Hf (wt %)	>95.3	>95.3	>95.3	97.2 - 97.6
Fe	99 - 123	131 - 165	140 - 175	290 - 300
O	110 - 253	126 - 265	220 - 250	270 - 370
Al	<50	<50	<50	30 - 38
C	<75	<75	<20	<30
Cu	<50	<50	<25	<40
H	<5	<5	<3	2.7 - 3.6
Mo	<10	19	<10	10 - 20
N	<50	<50	29 - 38	18 - 26
Nb	<50	<50	<50	<100
Ta	<100	<100	<100	<200
Ti	<50	<50	<25	33 - 37
U	<2	<2	<1	<0.5
W	<75	<75	<20	<20
Zr (wt %)	2.5 – 2.7	2.6 – 2.8	1.5 – 1.9	2.35 – 2.75
B	<0.5	<0.5	<0.5	Not Available
Cd	<2.5	<2.5	<2.5	
Co	<5	<5	<5	
Cr	<100	<100	<20	
Gd	<3.5	<3.5	<1	
Mn	<25	<25	<20	
Ni	<25	<25	<25	
P	<10	<10	<3	
Pb	<10	<10	<5	
Si	<25	<25	<25	
Sn	<10	<10	<10	
Th	<3.5	<3.5	<1	
V	<25	<25	<10	

Table 2
Specimen Size Configurations, (cm)

Configuration	Width	Length	Thickness
A	2.36	2.36	0.10
B	2.54	3.81	0.51
C	7.62	1.91	0.05

Table 3
Specimen Prefilming Conditions

Oxide prefilmed for 3-Days in 360°C water
Oxide prefilmed for 14-Days in 360°C water
Anodized at 60 Volts
No Prefilm

Table 4
Summary of Material and Test Conditions

Test	Group[6]	No. of Specs.	No. of Ingots	Temp, °C	Prefilm Conditions[5]	Test Environment	Sample Size
1	A	7	7	360	3-Day	Autoclave (pH 10)	(2)
2		2	2 of 7[1]		14-Day		
3		2	2 of 7[1]		Anodized		
4		3	3 of 7[1]		No Prefilm		
5	B	7	7	360	No Prefilm	Autoclave (pH 7)	(2)
6	C	30	1	360	No Prefilm	Autoclave (pH 7)	(3)
7	D	7	7	354	3-Day	ATR Out-of-Flux (pH 10)	(2)
8		2	2 of 7[1]		14-Day		
9		2	2 of 7[1]		Anodized		
10		3	3 of 7[1]		No Prefilm		
11	E	7	7	338	3-Day	Autoclave (pH 10)	(2)
12		2	2 of 7[1]		14-Day		
13		2	2 of 7[1]		Anodized		
14		3	3 of 7[1]		No Prefilm		
15	F	7	7	332	3-Day	ATR Out-of-Flux (pH 10)	(2)
16		2	2 of 7[1]		14-Day		
17		2	2 of 7[1]		Anodized		
18		3	3 of 7[1]		No Prefilm		
19	G	7	7	316	3-Day	Autoclave (pH 10)	(2)
20		2	2 of 7[1]		14-Day		
21		2	2 of 7[1]		Anodized		
22		3	3 of 7[1]		No Prefilm		
23	H	7	7	310	3-Day	ATR Out-of-Flux (pH 10)	(2)
24		2	2 of 7[1]		14-Day		
25		2	2 of 7[1]		Anodized		
26		3	3 of 7[1]		No Prefilm		
27	I	8	1	288	3-Day	Autoclave (pH 10)	(4)

Notes:
(1) n of the 7 ingots listed in Tests 1, 7, 11, 15, 19 and 23
(2) Configuration A, Table 2
(3) Configuration B, Table 2
(4) Configuration C, Table 2
(5) Days are in 360°C, pH 7 water
(6) The specimens associated with each of the tests in this group were tested in the same autoclave or ATR loop at the indicated temperature and pH.

Table 5
Summary of Pretransition Correlation Constants and Times-to-Transition

Test	Group	Pretransition Constants		Temp. (°C)	Time to Transition (days)	Time of Last Avg. Weight Gain, (days)	Normalized Pretransition Constants, k_c' (with n = 3), ($mg/dm^2/day$)	k_c ($= (k_c')^3$), $(mg/dm^2/day)^3$
		k''_c	n'					
1	A	1.42	3.06	360	189	185	1.37	2.57
2		1.42	3.07			196	1.36	2.52
3		1.42	3.07			196	1.36	2.52
4		1.53	2.98			182	1.55	3.72
5	B	1.55	2.95	360	193	112	1.59	4.02
6	C	1.67	3.26	360	180	180	1.45	3.05
7	D	1.49	3.44	354	212	183	1.19	1.69
8		1.51	3.42			186	1.22	1.82
9		1.69	3.25			178	1.48	3.24
10		1.47	3.49			176	1.15	1.52
11	E	1.08	3.00	338	409	368	1.08	1.26
12		1.00	3.10			366	0.94	0.83
13		1.15	2.94			374	1.20	1.73
14		1.14	2.95			364	1.18	1.64
15	F	0.84	2.77	332	396	249	0.98	0.94
16		0.81	2.8			252	0.92	0.78
17		0.99	2.6			238	1.31	2.25
18		0.77	2.86			396	0.85	0.61
19	G	0.70	2.88	316	1291	1200	0.77	0.46
20		0.68	2.90			1207	0.74	0.41
21		0.82	2.79			1178	0.98	0.94
22		0.75	2.83			1141	0.86	0.64
23	H	0.72	3.50	310	1473	1169	0.51	0.13
24		0.67	3.63			1218	0.44	0.09
25		0.87	3.21			1148	0.75	0.42
26		0.70	3.41			1102	0.53	0.15
27	I	0.42	2.95	288	4100	4098	0.44	0.09

Table 6
Summary of Posttransition Correlation Constants

Test	Temp. (°C)	Posttransition rate constants, k_L, (mg/dm^2/day)	Test	Temp. (°C)	Posttransition rate constants, k_L, (mg/dm^2/day)
1	360	0.05042	15	332	0.02440
2		0.04170	16		0.02414
3		0.04170	17		0.02825
4		0.05173	18		0.02517
5		0.03878	19	316	0.01675
6		*	20		0.01675
7	354	0.03151	21		0.02440
8		0.02622	22		0.01022
9		0.03372	23	310	*
10		0.03517	24		
11	338	0.02552	25		
12		0.02753	26		
13		0.01831	27	288	0.00327
14		0.02358			

Note: *Insufficient data to establish trend

Table 7
Ratios of the Hf-to-Zircaloy, Pretransition and Posttransition
Corrosion Rate Constants and the
Times-to-Transition at 100°C and 310°C

Temperature, °C	Ratio of the Hf to Zr Pretransition Rate Constants[1]	Ratio of the Hf to Zr Posttransition Rate Constants[2]	Ratio of the Hf to Zr Time-to-Transition[3]
100	0.05	0.75	76.7
310	0.18	0.20	2.55

Notes: (1) Ratio of Eqn. (6) to the cube root of Eqn. (3), Ref. (12)
(2) Ratio of Eqn. (7) to Eqn. (4), Ref. (12)
(3) Ratio of Eqn. (8) to Eqn. (6), Ref. (12)

Table 8
Tantalum and Lutetium Analyses, (wt. percent), [Reference (11)]

Specimen Number	Thermal Neutron Fluence (x 10^{20} nvt)	Surface		127 μm Depth		254 μm Depth		381 μm Depth		635 μm Depth	
		Ta	Lu	Ta	Lu	Ta	Lu	Ta	Lu	Ta	Lu
G-3-10	11.60	1.02	0.05	0.72	0.04	0.65	0.04	0.67	0.05	0.55	0.05
G-3-9	7.61	0.65	0.04	0.47	0.04	0.36	0.03	0.38	0.03	0.27	0.03
G-3-8	6.16	0.57	0.03	0.36	0.03	0.33	0.03	0.31	0.03	0.24	0.03
N-3-9	5.15	0.40	0.02	0.29	0.03	0.26	0.02	0.22	0.02	0.20	0.02
N-3-8	4.17	0.34	0.02	0.29	0.02	0.24	0.02	0.19	0.02	0.17	0.02

Table 9
Comparison of Measured and Predicted Oxide
Thicknesses for Hafnium Exposed Under Irradiated Conditions

Sample	Temp. (°C)	Exposure Time (Days)	Thermal Neutron Fluence (x10^{20} nvt)	Avg. Meas. Oxide Thickness (μm)	Range of Oxide Thicknesses Calculated by Eqn. (6) (μm)
1[1]	280	1100	4.17 – 11.60	0.27[2]	0.14 - 0.48
2	310	1903	190.8	0.64[3]	0.31 - 0.96
3	285	2749	55	<1.0[4]	0.22 - 0.71
4	298	765	83	<1.0[4]	0.18 - 0.58
5	254	3442	76	<0.5[4]	0.12 - 0.42

Notes: (1) From the Shippingport PWR Core 1 Control Rod [Reference (11)]
(2) Measured via X-Ray Absorption Technique
(3) Measured via SEM
(4) Less than the resolution of the hot-cell optical microscope

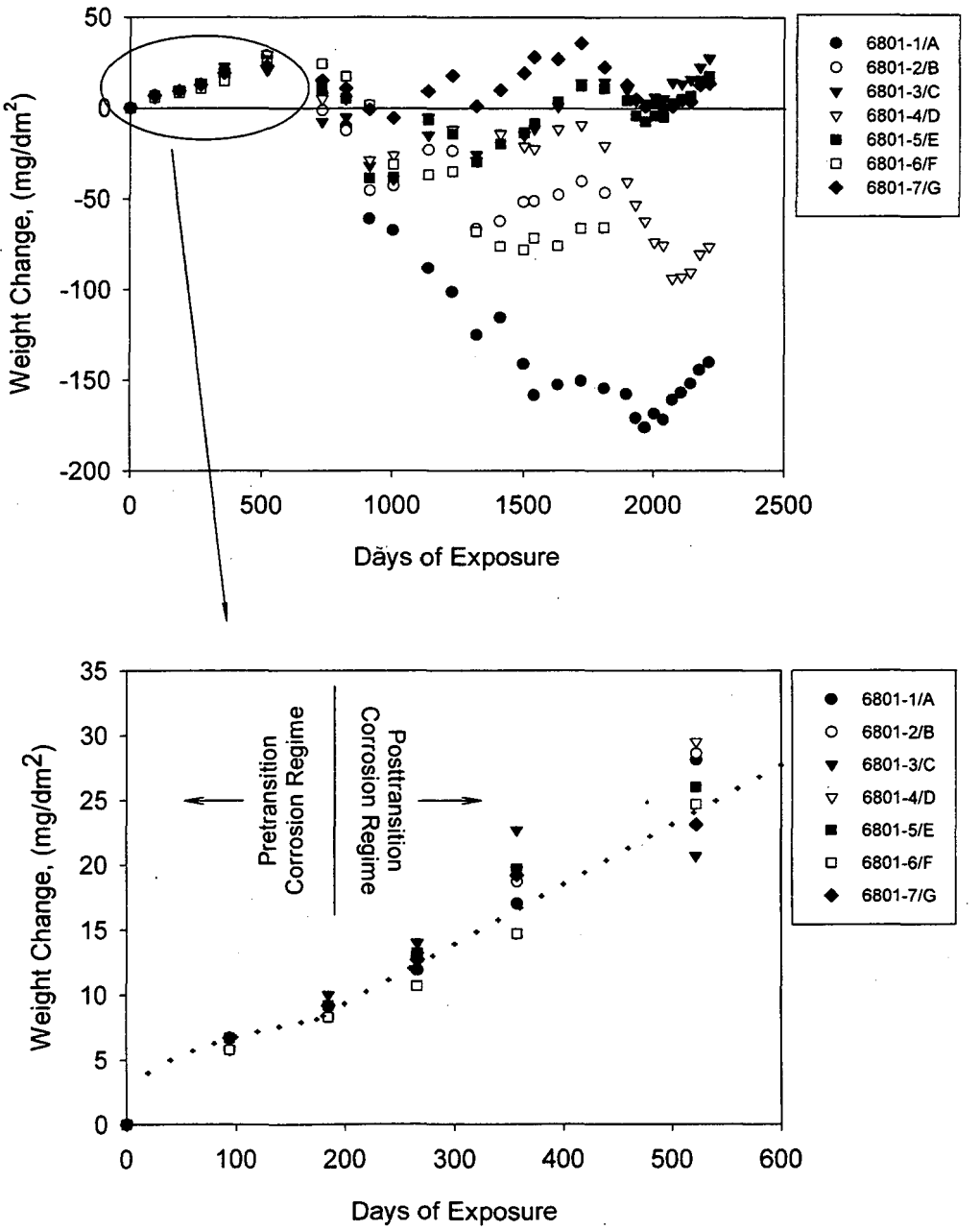

Figure 1 Corrosion behavior of hafnium in water at 360°C, with a room temperature adjusted pH of 10. The coupons had a 3-Day 360°C prefilm applied before the test. The data plotted in these figures are tabulated as Test 1 of this Appendix.

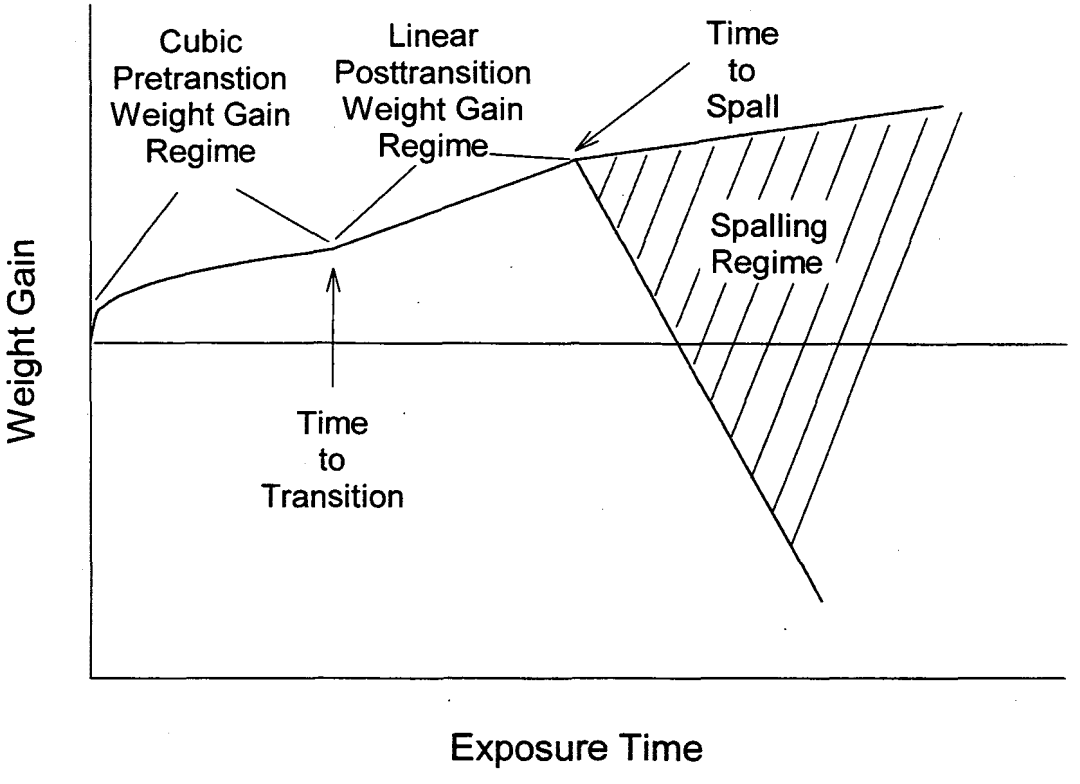

Figure 2 Schematic illustration of the three hafnium corrosion regimes and two transition points.

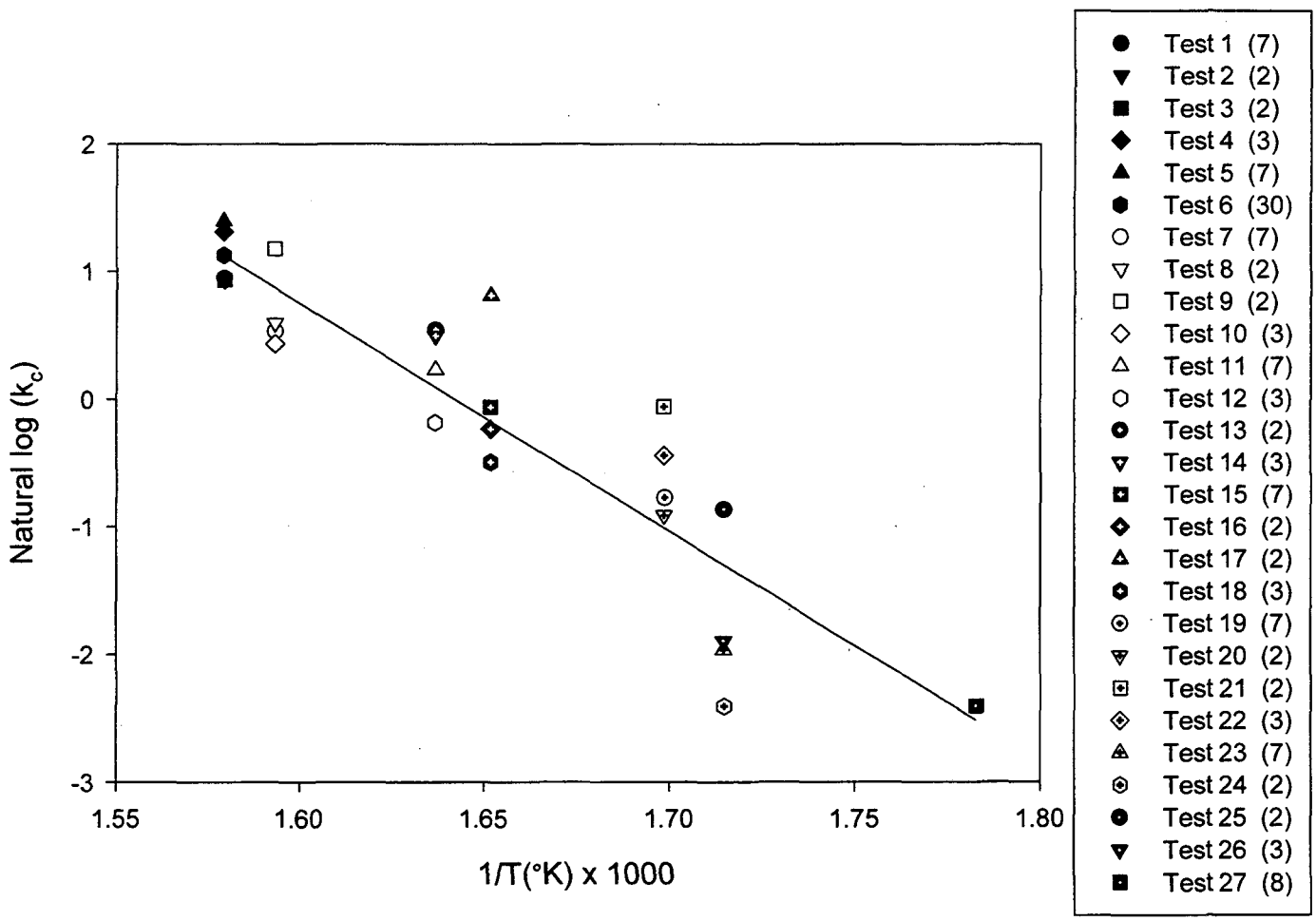

Figure 3 Natural logarithm of the pretransition hafnium corrosion rate constant, k_c, vs 1/Temperature (°K). The number in parentheses in the legend indicates the number of corrosion coupons included in the correlation.

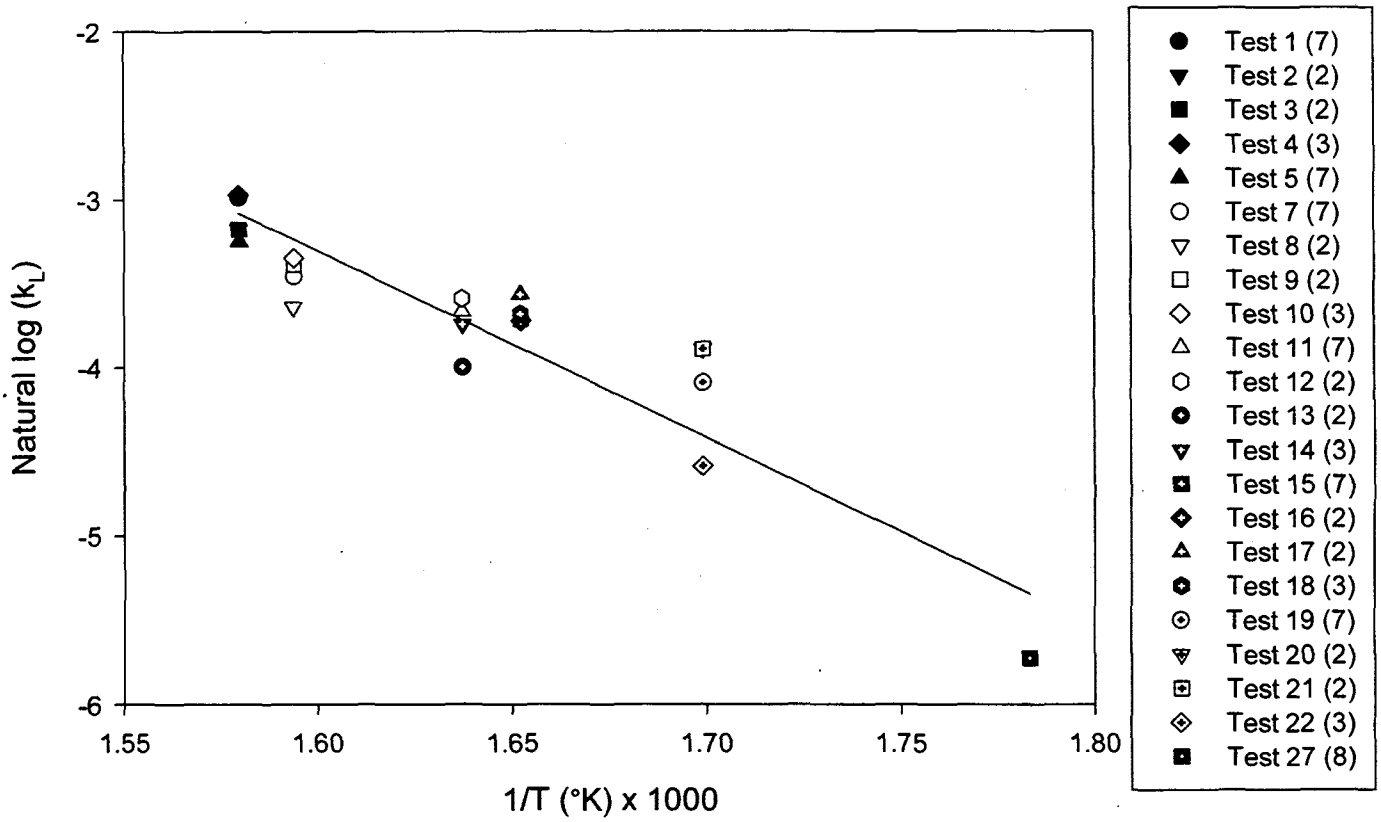

Figure 4 Natural logarithm of the posttransition hafnium corrosion rate constant, k_L, vs. 1/Temperature (°K). The number in parentheses in the legend indicates the number of corrosion coupons included in the correlation.

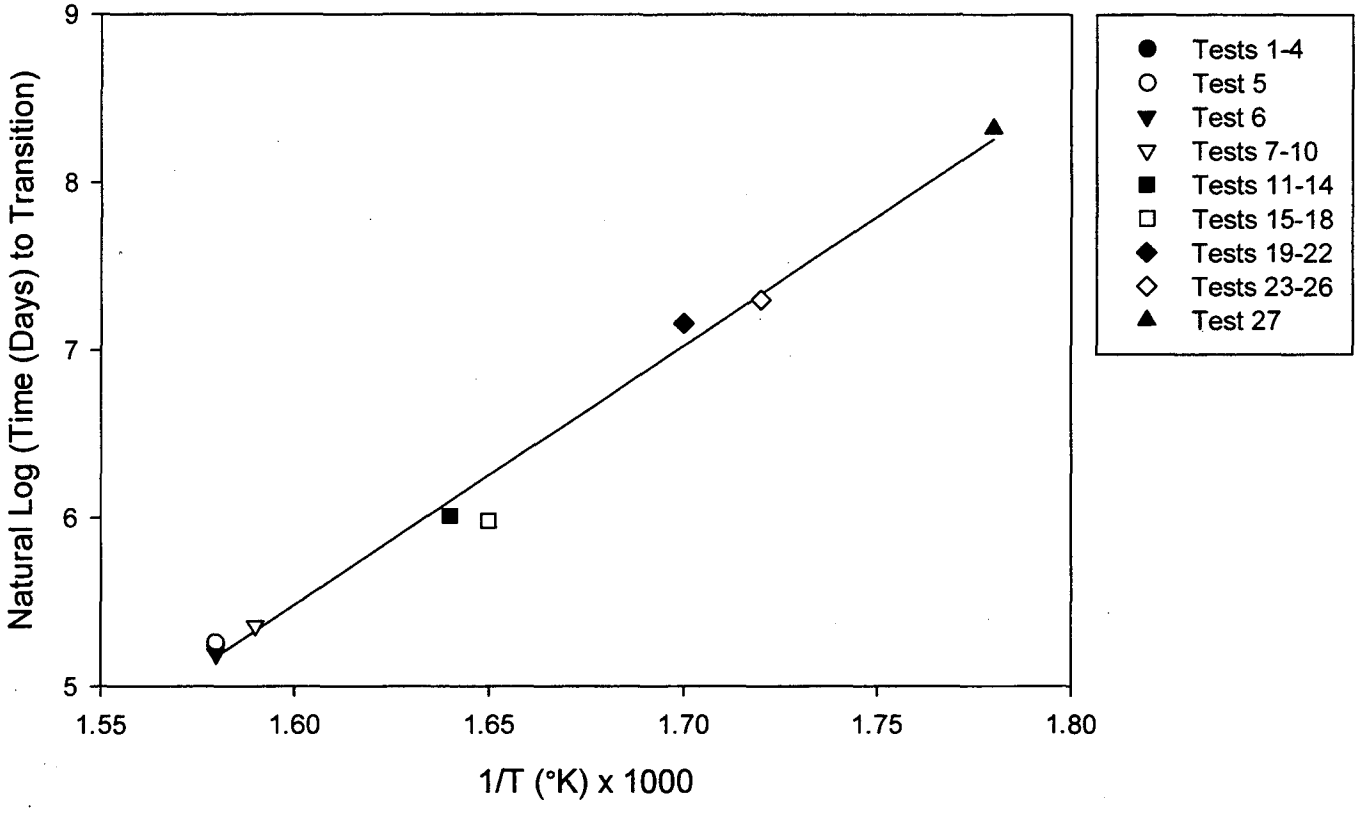

Figure 5 Time-to-Transition vs 1/T (°K).

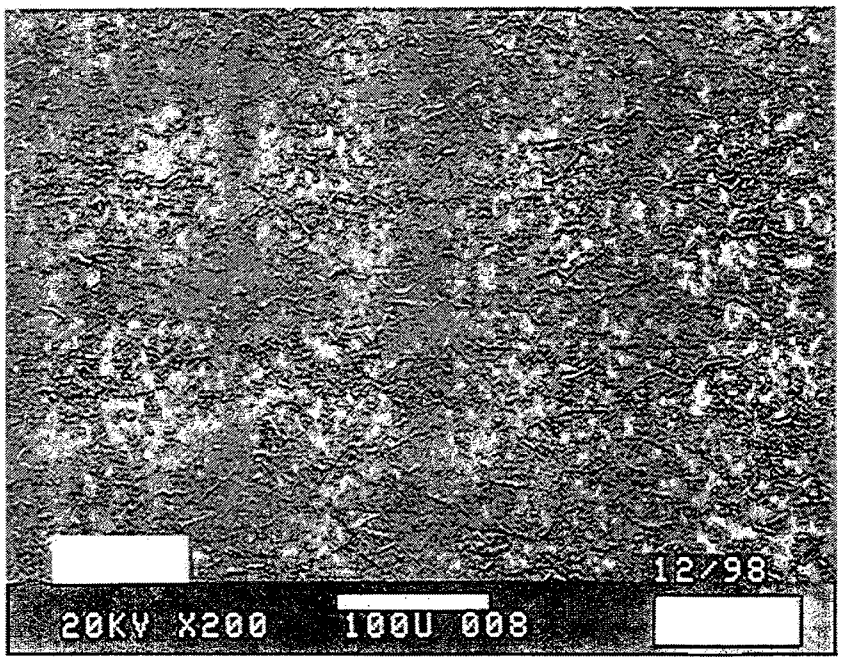

(a)

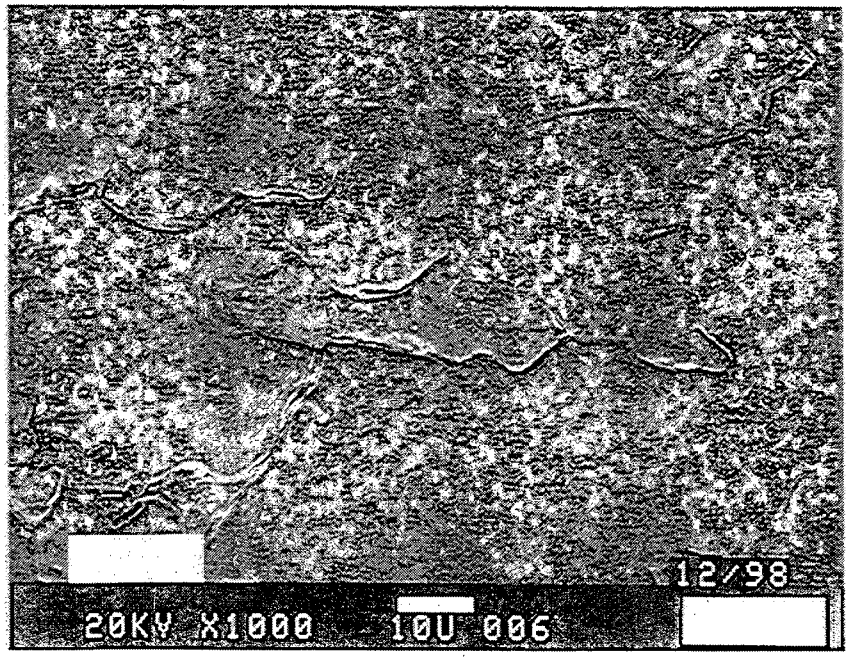

(b)

Figure 6 SEM micrographs of the surface of a pretransition oxide film as observed on a coupon that had been exposed in autoclave (pH 7) at 360°C for 125 days. A 3-day 360°C thermal prefilm had been applied prior to testing; (a) 200x Magnification, (b) 1000x Magnification.

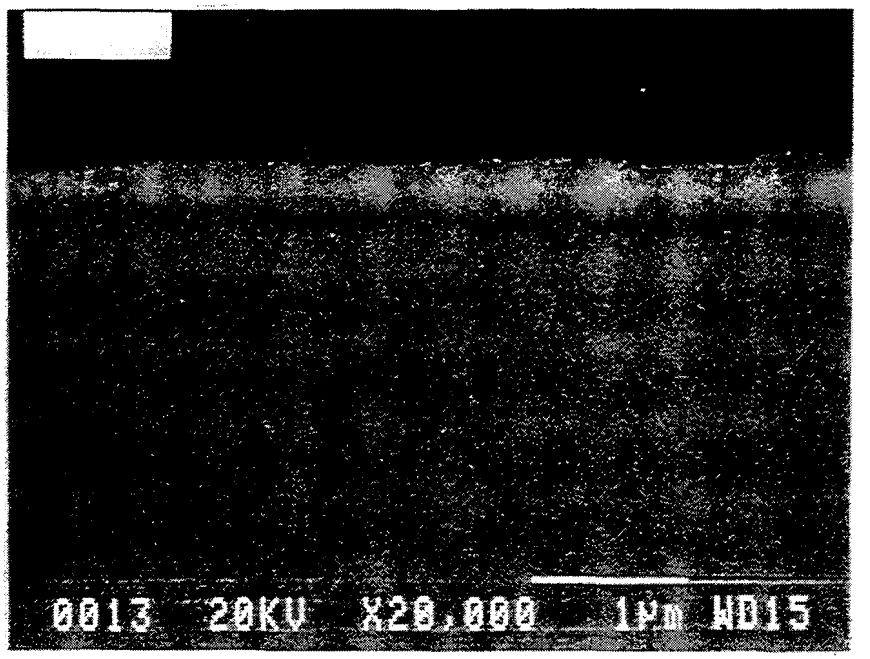

(a)

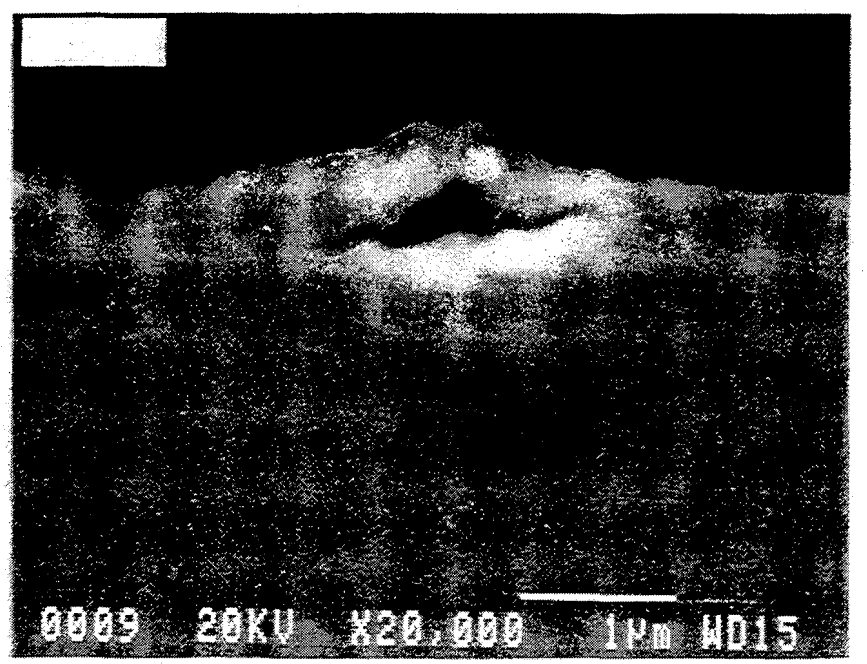

(b)

Figure 7 20,000x Magnification SEM cross-sectional micrographs of the pretransition oxide; (a) Example of the uniform, adherent oxide film. (b) Example of a nodule-like oxide feature.

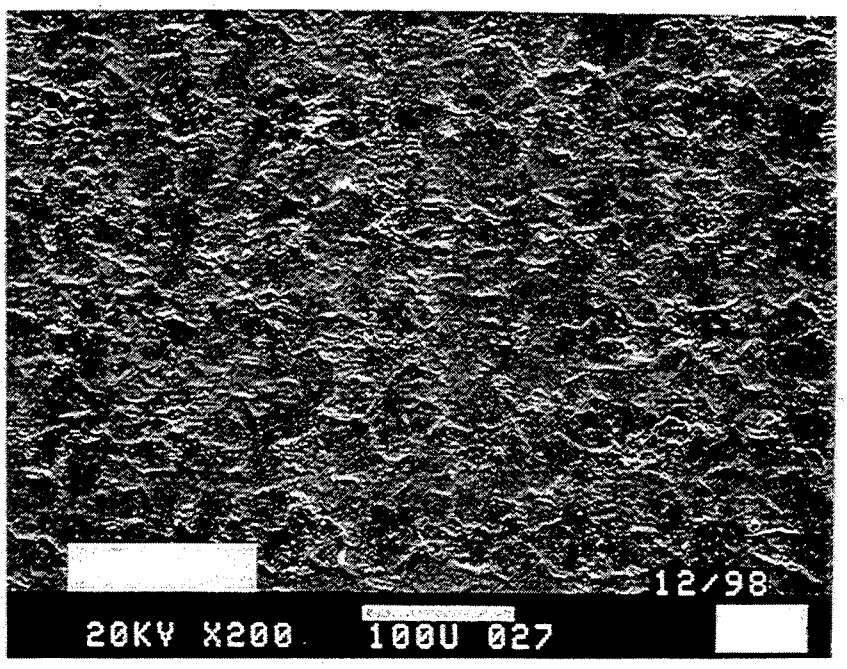

(a)

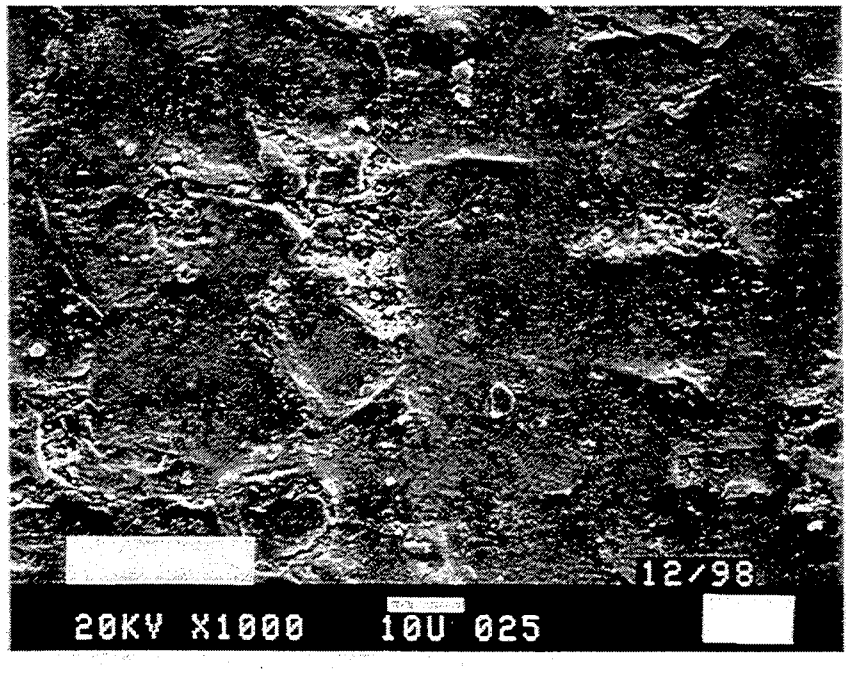

(b)

Figure 8 SEM micrographs of the surface of a posttransition oxide film on a coupon that was exposed in autoclave testing (pH 7) at 360°C for 540 days. No oxide prefilming was applied to the specimen prior to the test; (a) 200x Magnification, (b) 1000x Magnification.

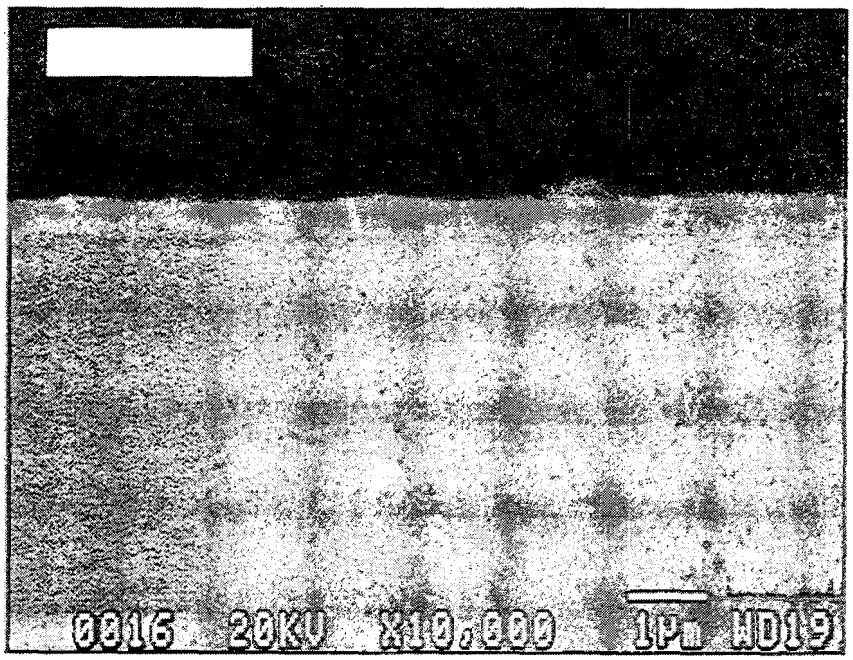

(a)

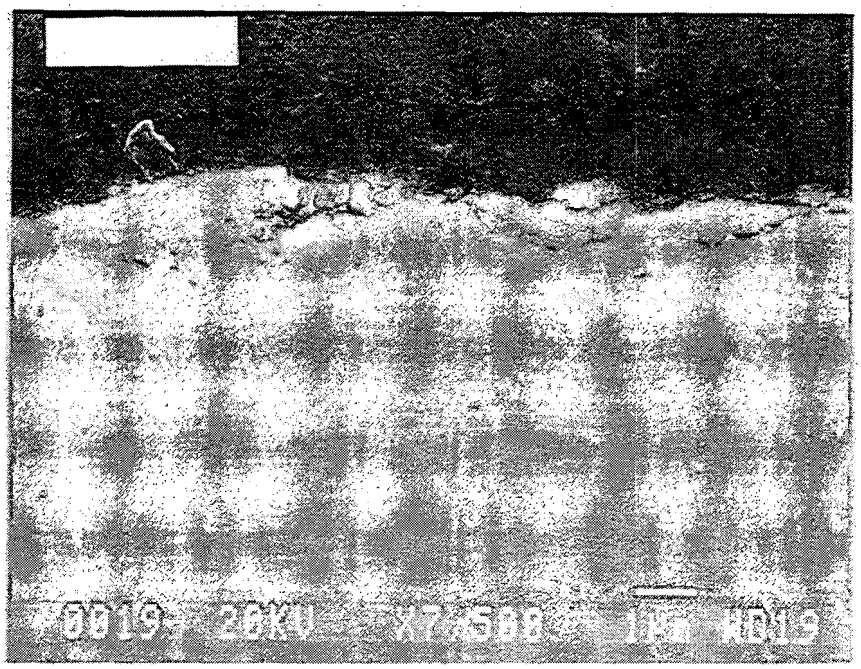

(b)

Figure 9 SEM cross-sectional micrographs of the posttransition oxide film that existed on the same coupon shown in Figure 8; (a) Example of the uniform, adherent oxide film, 10000x Magnification. (b) Example of a nodule-like oxide feature, 7500x Magnification.

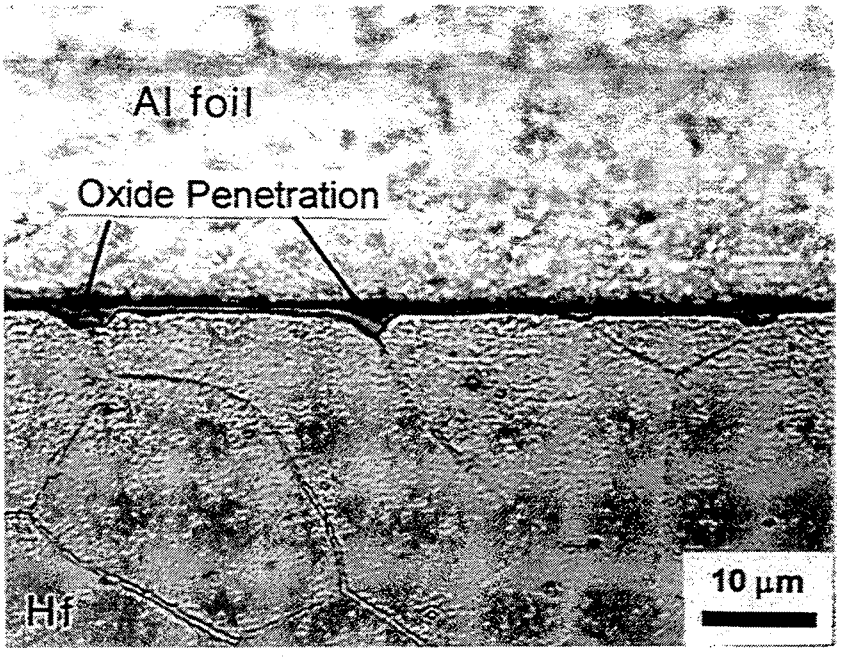

Figure 10 1500x optical micrograph of the posttransition of the coupon shown in Figures 8 and 9 (after etching) illustrating the nodule-like oxide features that penetrate along the hafnium metal grain boundaries.

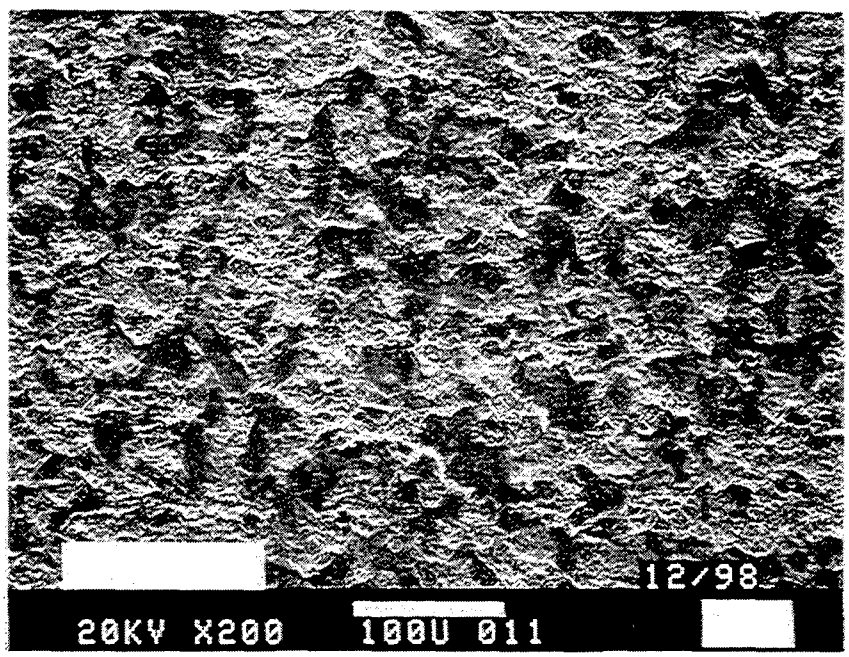

(a)

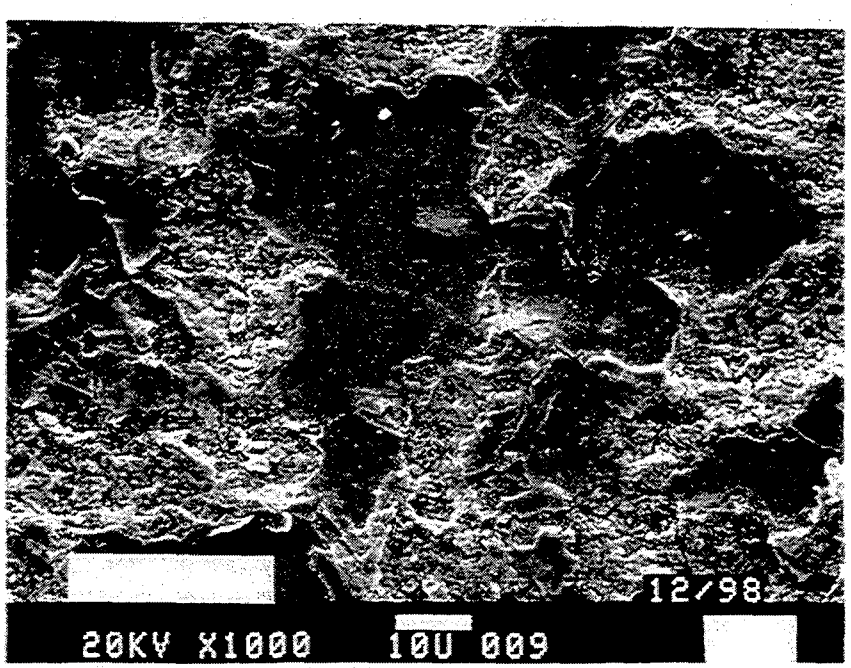

(b)

Figure 11 SEM micrographs of the surface of a spalling regime oxide film on a coupon that had been exposed in autoclave testing (pH 7) at 360°C for 731 days. No oxide prefilming was applied to the specimen prior to the test; (a) 200x Magnification, (b) 1000x Magnification.

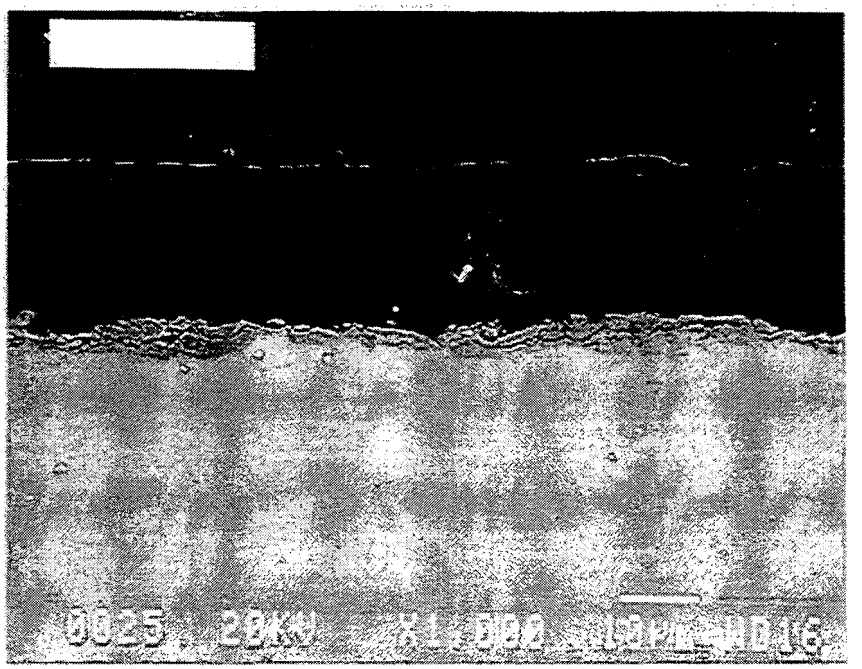

(a)

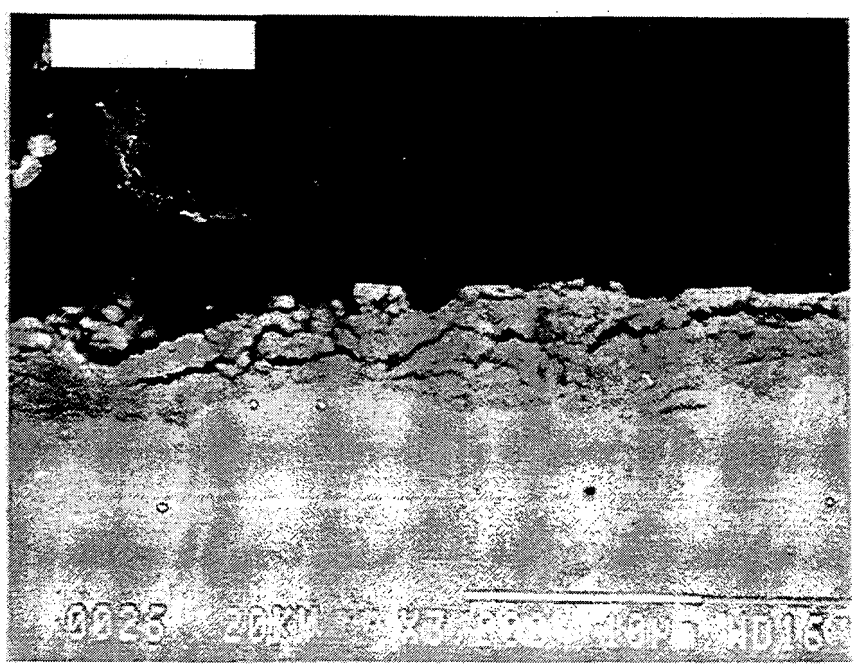

(b)

Figure 12 SEM cross-sectional micrographs of the spalling regime oxide film shown in Figure 11; (a) 1000x Magnification, (b) 3000x Magnification.

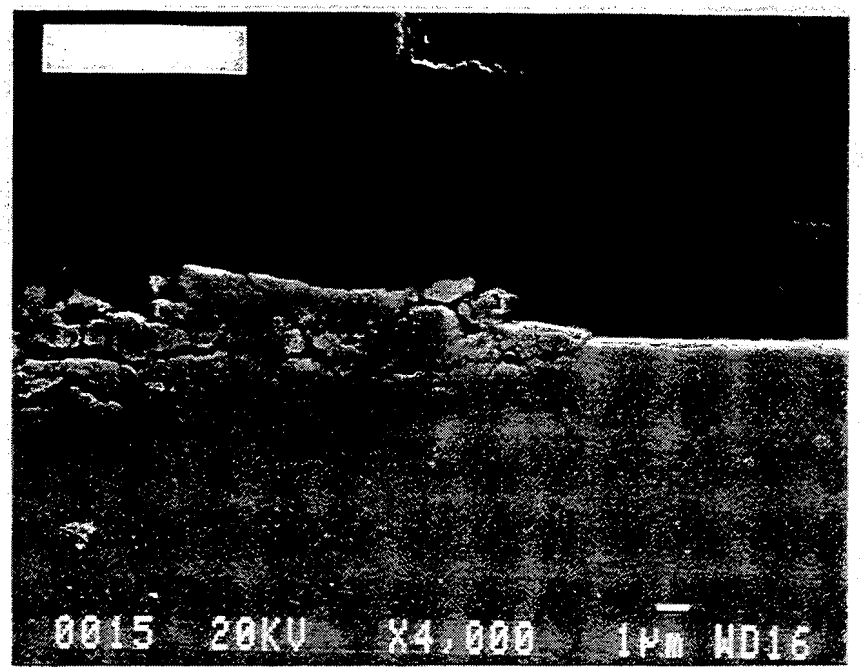

(a)

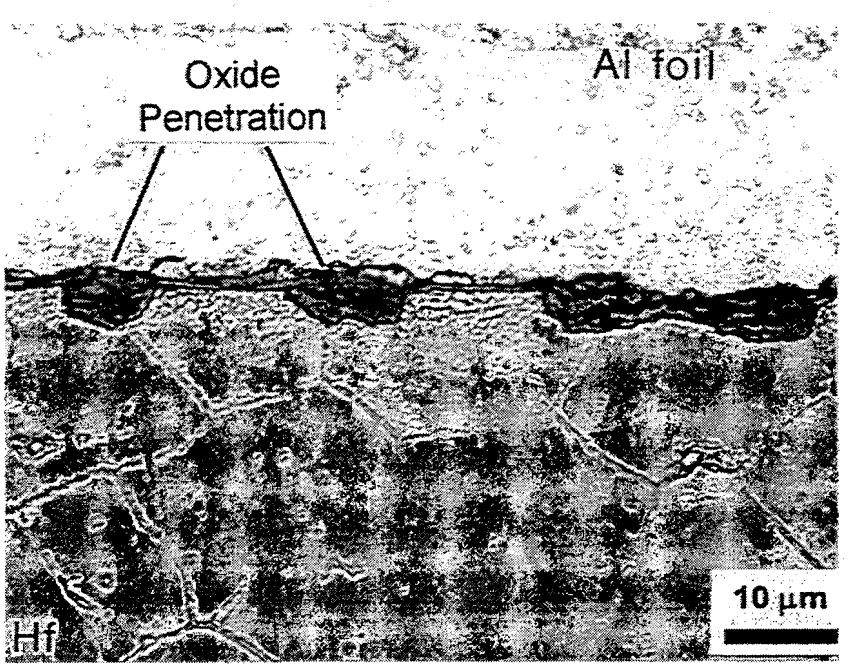

(b)

Figure 13 Spalling regime on the coupon shown in Figures 11 and 12, illustrating the growth of nodule-like oxide features; (a) 4000x SEM micrograph before etching, (b) 1500x optical micrograph after etching.

CORROSION DATA

Corrosion Kinetic Weight Gain Data, (mg/dm^2)[1]

Days of Exposure	Test 1 (360°C) Coupon/Ingot						
	6801-1/A	6801-2/B	6801-3/C	6801-4/D	6801-5/E	6801-6/F	6801-7/G
91	6.7	5.8	5.8	--	6.7	5.8	6.7
182	8.3	9.1	10.0	9.1	9.2	8.3	9.2
263	11.9	12.9	14.0	13.0	13.2	10.7	12.7
354	17.0	18.7	22.7	19.6	19.7	14.7	19.2
519	28.1	28.6	20.7	29.5	26.0	24.7	23.1
729	7.9	-1.5	-7.5	5.0	12.1	24.4	15.1
820	-10.0	-12.4	-5.3	4.8	5.4	17.5	10.8
911	-61.2	-45.5	-31.9	-28.8	-38.6	1.7	-0.9
1002	-67.4	-42.9	-39.2	-25.9	-38.1	-31.1	-5.5
1134	-88.1	-23.0	-14.8	-4.9	-6.6	-36.6	9.2
1226	-101.5	-23.7	-11.8	-12.0	-14.2	-34.9	17.8
1317	-125.2	-66.8	-25.8	-29.1	-29.6	-68.1	1.0
1408	-115.7	-62.4	-14.0	-14.4	-19.8	-76.2	9.7
1499	-141.4	-51.9	-14.9	-21.2	-13.6	-78.1	19.1
1539	-158.6	-51.5	-11.5	-22.5	-8.5	-71.7	28.0
1630	-152.7	-47.8	0.8	-11.7	3.5	-75.9	26.8
1721	-150.8	-40.6	13.7	-9.4	12.1	-66.2	35.6
1810	-154.6	-46.6	14.2	-20.7	10.9	-65.7	22.5
1895	-157.9	RFT[2]	10.0	-40.6	4.2	RFT	12.7
1930	-171.2		4.2	-53.2	-4.1		5.0
1965	-176.2		2.5	-62.3	-7.5		0.9
2001	-168.7		5.9	-73.9	-4.1		3.4
2036	-172.0		5.0	-75.6	-5.0		0.0
2071	-161.2		14.2	-93.9	2.5		0.9
2106	-157.1		13.3	-93.1	5.0		4.2
2141	-152.1		15.8	-90.6	6.7		3.4
2176	-144.6		22.5	-80.6	15.0		12.5
2211	-140.4		27.5	-76.4	17.6		13.4
Prefilm Weight Gain, mg/dm^2	2.7	2.1	2.6	2.6	3.3	3.1	2.2
Adjusted Days	3						

Days of Exposure	Test 2 (360°C)		Test 3 (360°C)		Test 4 (360°C)		
	Coupon/Ingot		Coupon/Ingot		Coupon/Ingot		
	6802-1/A	6802-2/E	6803-1/D	6803-2/G	6804-1/B	6804-2/C	6804-3/F
91	5.8	--	7.8	8.7	7.5	6.6	7.4
182	8.2	10.0	8.7	9.5	8.3	9.1	8.3
263	11.9	14.9	11.1	11.9	12.8	12.6	10.3
354	17.4	22.3	12.9	13.5	19.1	19.2	12.5
519	27.6	27.0	19.7	18.4	29.8	26.8	19.0
729	3.7	16.9	29.5	25.5	7.6	0.6	23.3
820	-11.2	12.9	34.1	33.4	4.5	-16.7	25.3
911	-79.9	5.5	21.6	41.1	-38.4	-37.1	12.1
1002	-84.1	10.6	14.8	37.5	-45.6	-45.2	6.2
1134	-87.0	39.9	13.8	59.4	-29.7	-30.6	7.7
1226	-96.5	34.5	1.7	51.4	-32.0	-35.6	-4.0
1317	-119.4	22.9	-11.0	39.6	-67.3	-62.9	-41.2
1408	-116.0	32.5	1.6	53.5	-58.2	-58.1	-32.2
1499	-152.9	39.0	-16.2	52.0	-73.9	-56.1	-58.4
1539	-168.6	47.6	-24.1	50.8	-81.0	-58.0	-60.3
1630	-159.8	53.0	-17.2	57.9	-66.3	-56.4	-47.7
1721	-151.7	66.5	-15.6	72.2	-52.5	-48.1	-38.7
1810	RFT	68.2	-13.9	RFT	-56.5	-52.2	-39.9
1895		57.4	-32.0		-59.0	-58.9	-37.4
1930		54.1	-48.5		-71.5	-69.7	-39.1
1965		45.8	RFT		-74.8	-76.3	-43.2
2001		48.3			-69.0	-75.5	-44.1
2036		49.1			-75.6	-77.1	-44.1
2071		47.4			-65.7	-69.7	-37.4
2106		50.7			-64.0	-67.2	-34.1
2141		51.6			-60.7	-65.5	-33.2
2176		59.9			-56.5	-58.9	-24.1
2211		64.0			-51.5	-53.9	-22.4
Prefilm Weight Gain, mg/dm^2	3.1	2.7	3.9	2.2	--	--	--
Adjusted Days	14				0		

Days of Exposure	Test 5[3] (360°C)						
	Coupon/Ingot						
	6805-1/A	6805-2/B	6805-3/C	6805-4/D	6805-5/E	6805-6/F	6805-7/G
56	5.9	5.1	6.1	5.2	6.1	6.0	6.0
112	6.7	6.8	6.9	6.9	7.8	6.8	6.8
168	10.1	11.1	10.4	11.2	11.3	7.7	8.6
252	11.8	14.6	11.9	13.4	12.8	10.0	11.5
336	15.3	17.6	16.1	19.2	17.9	12.0	13.2
420	18.6	19.6	19.1	22.0	21.6	14.7	16.0
504	18.5	16.2	17.4	15.6	20.0	15.4	17.1
588	14.3	15.3	--	6.9	19.1	18.8	18.8
672	0	-7.4	-11.7	-29.2	--	20.5	18.0
756	-8.4	-17.1	-20.1	-32.8	-11.3	19.8	15.3

	Test 6[3] (360°C)					
Days of Exposure	Coupon/Ingot					
	6806-1/H	6806-2/H	6806-3/H	6806-4/H	6806-5/H	6806-6/H
28	4.9	4.9	5.3	5.3	4.9	5.3
56	5.7	6.0	6.0	6.4	5.7	6.0
120	7.6	7.9	7.9	7.9	7.6	7.9
180	8.7	8.7	8.7	9.8	9.1	8.7
240	12.3	11.9	12.2	12.5	12.0	11.8
300	12.1	12.8	12.8	12.4	12.1	11.7
360	13.2	13.6	13.9	14.0	13.6	12.5
405	13.9	14.1	13.3	14.1	14.1	11.9
478	14.0	13.9	13.2	13.6	12.1	11.9
601	RFT	15.1	15.8	15.8	14.4	14.0
Days of Exposure	Coupon/Ingot					
	6806-7/H	6806-8/H	6806-9/H	6806-10/H	6806-11/H	6806-12/H
28	5.3	4.9	4.9	4.5	4.9	4.9
56	5.6	5.7	6.4	6.0	5.7	6.0
120	7.5	7.2	7.6	7.6	7.5	7.5
180	8.3	7.9	8.3	8.7	8.7	9.1
240	12.0	11.2	12.0	11.3	11.7	12.5
300	11.6	11.7	12.1	12.1	11.3	12.8
360	12.8	12.1	12.9	12.5	14.0	13.6
405	13.2	12.3	12.9	12.7	12.7	12.0
478	12.4	11.7	12.9	12.1	12.5	12.1
601	12.0	14.0	14.4	14.4	12.8	10.6
Days of Exposure	Coupon/Ingot					
	6806-13/H	6806-14/H	6806-15/H	6806-16/H	6806-17/H	6806-18/H
28	4.9	4.5	4.9	4.9	5.3	4.6
56	5.7	5.3	6.0	5.7	5.3	5.3
120	7.2	6.8	7.9	7.5	6.8	6.8
180	8.7	8.3	8.3	8.3	8.7	8.0
240	12.1	11.9	11.7	11.5	11.3	11.0
300	12.5	13.2	12.1	12.5	11.8	10.6
360	12.5	13.2	13.2	13.6	12.2	12.9
405	11.6	12.8	13.3	13.4	12.5	13.1
478	11.0	11.7	14.0	12.8	12.2	13.7
601	6.1	RFT	14.3	12.8	11.4	13.7
Days of Exposure	Coupon/Ingot					
	6806-19/H	6806-20/H	6806-21/H	6806-22/H	6806-23/H	6806-24/H
28	4.6	4.6	4.6	4.2	4.6	4.6
56	5.3	5.3	5.0	4.2	5.1	5.1
120	6.8	6.8	6.3	6.3	7.6	7.2
180	7.6	7.6	7.6	8.0	8.4	8.4
240	9.5	10.6	10.3	9.7	10.0	10.1
300	9.9	12.5	11.5	10.6	11.4	11.9
360	12.6	13.3	13.2	11.9	12.3	12.8
405	12.4	12.8	13.1	11.7	12.5	12.6
478	11.4	9.1	13.0	11.7	13.0	13.9
601	11.0	RFT	13.0	12.6	11.8	12.7
Days of Exposure	Coupon/Ingot					
	6806-25/H	6806-26/H	6806-27/H	6806-28/H	6806-29/H	6806-30/H
28	4.6	4.6	4.2	4.6	4.6	4.6
56	4.6	5.0	4.2	4.6	4.6	5.0
120	6.7	7.2	5.9	7.6	7.2	7.1
180	8.0	8.4	6.7	8.0	8.0	8.4
240	10.2	10.4	8.6	10.2	10.2	10.3
300	10.9	12.5	9.4	10.7	11.9	11.8
360	12.3	7.6	12.0	11.7	13.0	12.7
405	13.2	11.3	11.3	11.3	13.1	12.4
478	13.5	11.8	12.2	11.8	13.9	13.0
601	11.4	10.1	10.9	9.3	13.5	10.9

Days of Exposure	Test 7 (354°C)						
	Coupon/Ingot						
	6701-1/A	6701-2/B	6701-3/C	6701-4/D	6701-5/E	6701-6/F	6701-7/G
86	5.8	4.1	5.7	4.8	10.7	4.7	4.1
176	6.2	6.7	6.0	6.5	6.0	7.4	7.2
285	8.3	7.8	7.5	7.9	7.5	8.0	7.9
344	11.5	11.4	11.3	9.9	8.7	10.0	9.9
423	13.3	12.6	12.6	10.6	13.1	13.6	10.4
533	18.4	18.5	17.2	13.7	14.0	16.0	13.4
615	8.4	7.7	6.4	5.4	6.6	9.3	9.2
790	6.7	7.7	3.9	3.7	5.7	9.3	9.2
Prefilm Weight Gain, mg/dm^2	2.8	2.7	2.3	2.5	2.6	3.0	2.8
Adjusted Days	7.3						

Days of Exposure	Test 8 (354°C)		Test 9 (354°C)		Test 10 (354°C)		
	Coupon/Ingot		Coupon/Ingot		Coupon/Ingot		
	6702-1/A	6702-2/E	6703-1/D	6703-2/G	6704-1/B	6704-2/C	6704-3/F
86	7.8	4.5	5.8	9.1	2.7	10.3	6.2
176	5.6	7.7	7.9	8.6	6.0	5.2	6.3
285	7.9	7.8	8.6	9.1	7.3	6.7	6.8
344	11.0	9.7	11.5	10.7	10.7	9.8	8.6
423	11.6	10.9	13.0	12.5	13.0	12.2	10.3
533	15.2	14.3	18.7	16.2	17.6	15.6	14.5
615	6.9	7.7	8.7	9.6	7.7	4.8	7.9
790	4.4	7.7	10.4	11.2	6.0	4.0	8.7
Prefilm Weight Gain, mg/dm^2	2.8	3.2	1.3	2.2	–	–	–
Adjusted Days	10.3		2.2		0		

Days of Exposure	Test 11 (338°C)						
	Coupon/Ingot						
	6401-1/A	6401-2/B	6401-3/C	6401-4/D	6401-5/E	6401-6/F	6401-7/G
91	3.6	4.5	5.4	3.6	4.5	5.4	4.5
182	5.0	5.8	6.8	5.0	5.8	6.6	5.8
273	5.8	6.6	7.7	6.6	8.3	7.5	6.7
364	8.0	9.0	10.1	8.5	9.0	9.1	9.4
455	9.2	10.0	11.2	10.0	10.6	10.6	10.6
544	10.0	13.1	13.0	12.4	12.4	11.5	13.2
635	12.4	15.4	15.3	13.9	14.7	13.0	14.9
726	13.8	16.9	17.9	16.3	--	14.6	17.4
817	15.3	20.4	20.3	19.3	19.6	16.2	20.7
908	19.2	23.4	23.4	23.1	24.5	19	24.4
999	22.8	22.9	--	27.5	26.5	22.9	28.9
1090	26.8	22.8	27.5	31.1	28.2	24.7	29.1
1181	21.6	16.3	21.8	26.5	24.2	26.7	31.0
1272	20.9	17.5	20.5	29.1	18.9	28.4	39.1
1363	24.3	21.9	22.1	29.5	14.8	31.0	29.8
1454	13.6	10.1	-3.2	23.7	4.1	26.8	32.7
1545	13.5	0.2	0.0	16.1	4.3	23.6	26.8
1636	10.4	-2.4	-10.1	14.7	0.3	26.4	28.6
1727	-5.1	-5.3	-12.8	7.9	-13	14.3	26.6
1797	-5.0	0.8	-9.1	11.6	-9.2	10.0	38.3
1890	-11.3	-3.9	-5.8	16.0	-7.5	7.1	32.0
1980	-34.0	-9.1	-5.8	18.3	-5.8	5.8	37.5
2055	-29.9	-10.8	-4.2	12.5	-10.0	-6.6	39.1
2134	-38.1	-8.3	0.0	17.5	-4.2	-5.8	32.5
2225	-36.5	-16.6	-12.5	10.8	-6.7	-12.5	35.8
2316	-37.6	-25.3	-13.1	11.9	-4.2	-12.8	38.7
Prefilm Weight Gain, mg/dm^2	0.9	0.9	1.8	1.8	1.8	2.7	2.7
Adjusted Days	4.9						

Days of Exposure	Test 12 (338°C)		Test 13 (338°C)		Test 14 (338°C)		
	Coupon/Ingot		Coupon/Ingot		Coupon/Ingot		
	6402-1/A	6402-2/E	6403-1/D	6403-2/G	6404-1/B	6404-2/C	6404-3/F
91	2.7	4.5	4.5	6.5	5.4	4.5	5.4
182	4.2	5.8	5.8	7.8	7.2	5.8	6.7
273	5.0	7.5	6.6	7.8	8.4	6.6	6.7
364	7.8	8.9	9.2	10.2	9.7	9.0	9.0
455	9.5	10.3	10.6	10.6	10.8	10.0	10.2
544	11.3	12.4	14.4	11.4	12.3	13.1	11.5
635	13.5	14.5	17.5	11.5	13.9	15.4	12.0
726	15.6	17.1	20.5	12.0	15.2	16.9	13.7
817	17.8	20.5	23.5	12.6	17.9	20.4	15.4
908	21.8	24.4	26.9	13.6	21.2	23.4	18.1
999	22.4	27.2	28.0	15.0	23.7	22.9	20.4
1090	22.9	29.8	23.6	19.8	29.0	22.8	24.5
1181	10.7	23.4	13.6	17.6	24.3	16.3	25.0
1272	13.4	20.0	8.1	18.9	23.6	17.5	26.9
1363	13.2	16.4	9.8	22.2	23.2	21.9	29.4
1454	-16.9	6.8	-0.5	26.2	3.9	10.1	26.7
1545	-20.7	1.4	49.2	25.7	-2.6	0.3	25.1
1636	-19.2	5.9	53.8	31.5	-1.8	-2.3	26.3
1727	-40.3	1.8	57.5	31.7	-4.9	-13.2	15.6
1797	-45.0	1.7	63.2	36.4	-10.7	-13.0	8.4
1890	-45.5	8.3	58.7	39.7	-14.7	-14.9	8.4
1980	-63.3	8.3	45.9	42.4	-24.0	-24.6	6.7
2055	-60.8	5.8	47.6	42.4	RFT	-27.9	-2.4
2134	-63.3	9.2	56.2	47.6		-28.7	-6.6
2225	-66.6	1.7	53.7	45.0		-32.1	-21.5
2316	-63.0	6.8	55.0	49.9		-43.4	-23.4
Prefilm Weight Gain, mg/dm^2	0.9	1.8	2.7	1.8	--	--	--
Adjusted Days	2.3		10.3		0		

Days of Exposure	Test 15 (332°C) Coupon/Ingot						
	6301-1/A	6301-2/B	6301-3/C	6301-4/D	6301-5/E	6301-6/F	6301-7/G
91.7	3.5	4.0	3.7	3.2	4.3	3.9	3.5
223.4	6.6	7.0	7.7	6.5	6.9	7.2	7.7
396.4	7.2	7.2	7.2	9.5	8.0	8.0	8.8
785.8	16.4	15.2	16.1	19.1	18.2	19.1	18.5
905.7	10.1	9.5	11.6	13.6	13.2	12.5	11.6
1073.7	9.2	10.3	9.1	11.1	10.7	11.7	9.9
1209.8	3.4	6.2	4.1	7.8	8.2	8.4	9.9
1361.4	2.6	3.7	3.2	3.7	8.2	9.2	9.1
1584.9	7.6	9.5	5.7	6.2	8.2	9.2	13.2
Prefilm Weight Gain, mg/dm^2	2.9	2.7	2.9	2.6	2.8	3.2	2.6
Adjusted Days	25.8						

Days of Exposure	Test 16 (332°C) Coupon/Ingot		Test 17 (332°C) Coupon/Ingot		Test 18 (332°C) Coupon/Ingot		
	6302-1/A	6302-2/E	6303-1/D	6303-2/G	6304-1/B	6304-2/C	6304-3/F
91.7	4.0	3.2	4.5	6.4	2.9	3.2	2.8
223.4	6.6	6.6	8.1	9.7	5.6	6.1	7.0
396.4	7.5	7.6	8.3	11.3	6.2	6.2	6.7
785.8	16.4	17.5	17.4	24.1	15.3	15.1	18.1
905.7	10.2	12.1	14.2	18.7	10.6	9.8	12.0
1073.7	7.7	11.3	12.5	19.6	9.7	9.0	11.1
1209.8	5.2	3.7	14.2	20.4	4.7	4.8	7.8
1361.4	1.9	2.0	10.7	16.1	2.2	4.0	6.2
1584.9	4.4	-0.5	16.8	17.8	5.6	9.0	8.6
Prefilm Weight Gain, mg/dm^2	3.0	2.9	2.3	2.3	–	–	–
Adjusted Days	28.9		14.7		0		

Days of Exposure	Test 19 (316°C)						
	Coupon/Ingot						
	6001-1/A	6001-2/B	6001-3/C	6001-4/D	6001-5/E	6001-6/F	6001-7/G
91	3.3	2.5	2.5	2.5	2.5	3.3	2.5
182	3.3	3.3	3.3	4.2	4.2	4.2	3.3
273	4.2	5.0	4.2	4.2	5.0	5.0	4.2
483	6.4	6.8	6.2	6.3	7.0	7.0	6.6
595	6.7	7.2	6.2	6.3	7.0	6.9	7.2
777	7.4	8.6	7.9	8.2	8.2	8.4	8.2
959	9.0	9.7	9.8	9.6	9.7	9.4	9.9
1141	10.5	11.5	11.9	10.7	11.0	10.7	11.6
1410	14.0	15.8	17.5	15.3	14.6	14.2	17.1
1592	16.2	19.1	21.4	18.1	16.7	15.0	20.0
1774	20.6	23.3	25.9	21.0	18.8	14.7	28.1
1876	21.6	27.4	27.4	24.1	24.2	20.0	27.5
2058	25.8	29.3	30.8	28.3	27.1	24.1	31.7
2240	28.2	34.4	33.4	RFT	31.8	28.5	39.1
2333	31.5	37.4	38.2		35.9	31.6	44.1
2879	30.7	49.0	25.8		32.6	34.9	50.8
3047	17.4	34.9	8.3		9.2	14.1	47.5
Prefilm Weight Gain, mg/dm^2	2.9	2.7	2.6	2.5	2.9	3.1	2.9
Adjusted Days	59.4						

Days of Exposure	Test 20 (316°C)		Test 21 (316°C)		Test 22 (316°C)		
	Coupon/Ingot		Coupon/Ingot		Coupon/Ingot		
	6002-1/A	6002-2/E	6003-1/D	6003-2/G	6004-1/B	6004-2/C	6004-3/F
91	2.5	2.5	4.3	4.3	1.7	5.8	2.5
182	2.5	3.3	6.1	5.2	2.5	7.4	2.5
273	5.0	4.2	6.9	6.1	4.2	7.4	4.2
483	5.7	6.3	8.5	8.3	5.3	9.9	6.3
595	6.5	6.7	8.1	8.3	5.7	10.1	6.3
777	7.6	8.4	9.2	8.9	6.8	11.2	7.2
959	9.0	9.7	10.1	9.7	8.2	12.7	8.1
1141	11.0	12.1	10.7	10.6	9.4	13.5	9.3
1410	14.8	16.8	12.5	12.5	12.6	15.9	11.5
1592	17.9	20.2	13.6	12.1	15.0	17.6	12.0
1774	23.7	22.0	13.2	13.6	19.5	20.5	12.4
1876	23.3	26.7	17.3	14.7	20.8	23.2	17.5
2058	27.5	30.6	17.9	15.6	24.1	26.9	18.7
2240	30.2	33.2	21.0	18.0	28.8	30.8	21.6
2333	32.5	37.6	24.2	19.9	30.8	33.1	24.1
2879	20.8	30.1	33.8	26.8	24.9	26.5	28.3
3047	12.5	1.7	36.3	27.7	2.5	7.5	22.4
Prefilm Weight Gain, mg/dm^2	2.7	3.0	3.1	1.7	–	–	–
Adjusted Days	66.0		37.4		0		

Days of Exposure	Test 23 (310°C)						
	Coupon/Ingot						
	5901-1/A	5901-2/B	5901-3/C	5901-4/D	5901-5/E	5901-6/F	5901-7/G
220	3.2	3.7	4.3	3.1	3.1	4.2	3.6
317	4.2	4.3	3.7	3.9	4.4	5.1	4.0
540	4.7	4.4	3.8	3.7	4.0	5.5	4.5
1102	5.5	5.2	4.0	6.2	4.7	5.9	5.1
1495	5.5	5.2	4.0	3.7	4.7	5.1	4.2
1927	6.3	6.1	4.8	4.5	5.5	6.7	5.9
2414	7.2	6.9	9.8	7.8	8.0	8.4	7.6
2662	8.0	8.6	8.1	7.0	8.8	8.4	7.6
Prefilm Weight Gain, mg/dm^2	3.1	2.5	2.6	2.3	2.3	3.1	2.4
Adjusted Days	67.1						

Days of Exposure	Test 24 (310°C)		Test 25 (310°C)		Test 26 (310°C)		
	Coupon/Ingot		Coupon/Ingot		Coupon/Ingot		
	5902-1/A	5902-2/E	5903-1/D	5903-2/G	5904-1/B	5904-2/C	5904-3/F
220	2.9	3.2	4.7	5.2	2.7	2.2	3.7
317	3.3	4.2	6.2	6.1	3.0	3.3	4.2
540	3.8	4.2	5.7	6.8	3.8	3.7	4.4
1102	4.1	5.6	6.8	7.4	5.8	6.6	5.2
1495	4.1	3.9	5.0	6.5	4.2	1.6	3.5
1927	4.9	5.6	5.9	7.4	5.0	4.1	4.3
2414	7.4	8.1	8.5	9.1	6.6	6.6	6.0
2662	7.4	7.2	7.6	9.1	8.3	5.7	5.2
Prefilm Weight Gain, mg/dm^2	2.9	3.3	2.7	1.9	--	--	--
Adjusted Days	115.7		45.9		0		

Days of Exposure	Test 27 (288°C) Coupon/Ingot 5501-1/I	5501-2/I	5501-3/I	5501-4/I	5501-5/I	5501-6/I	5501-7/I	5501-8/I
166	2.6	3.2	3.5	3.8	3.8	3.5	4.4	2.8
278	2.6	3.8	3.2	4.4	3.5	3.8	4.6	2.8
493	3.5	4.3	4.3	4.6	4.9	3.8	5.2	3.4
533	3.5	3.8	4.0	4.6	4.3	4.1	5.5	3.7
722	3.8	4.3	4.3	5.2	5.2	4.9	6.1	4.3
1327	4.9	5.2	5.2	5.8	5.5	5.8	6.6	5.1
1471	4.9	4.9	5.2	4.6	5.8	4.9	6.4	4.3
1730	5.2	5.8	5.5	5.5	5.8	5.5	6.6	4.3
2025	5.5	6.0	6.3	5.8	7.3	6.3	7.5	5.7
2410	4.3	4.6	4.6	5.2	5.2	4.9	5.8	4.3
2627	5.5	5.8	6.0	6.1	6.3	5.8	7.2	5.1
3031	6.0	6.3	6.3	6.4	6.3	6.1	8.1	4.8
3331	6.3	6.3	6.6	6.6	6.1	6.6	8.4	5.7
3831	7.5	7.8	8.0	7.8	7.2	8.1	8.9	6.8
4013	9.2	8.9	9.7	8.9	8.9	8.9	10.3	8.6
4195	9.7	8.9	10.3	9.7	9.7	10.0	11.2	9.2
4377	9.7	8.6	10.0	8.9	8.9	9.2	10.6	8.6
4559	10.9	9.5	11.2	9.7	9.7	9.7	10.8	10.0
4642	10.6	9.7	11.5	9.7	10.3	10.9	12.0	10.0
4824	11.5	10.3	12.0	10.6	10.6	11.2	11.8	10.9
4946	11.2	10.3	12.6	10.0	10.3	11.2	12.0	10.3
5128	12.6	11.5	13.5	11.5	11.8	12.0	12.9	12.0
5313	12.3	10.6	13.2	11.2	11.2	11.2	12.9	11.2
5398	12.9	12.0	14.3	12.0	12.6	12.6	13.8	12.3
5489	13.8	12.3	14.6	12.3	12.6	12.9	14.0	12.6
5677	15.2	13.8	15.2	13.5	13.8	14.0	15.2	13.7
5934	17.2	15.2	3.5	14.9	16.0	15.2	17.2	15.2
Prefilm Weight Gain, mg/dm^2	2.6	2.6	2.6	3.2	2.9	2.9	3.2	1.4
Adjusted Days	267.1							

Note: (1) All weight gains and losses are referenced to the non-prefilmed condition.
(2) RFT≡ Removed from test
(3) No prefilm applied